BRANCHED GDGTS AS TRACER OF SOIL ORGANIC MATTER TRANSPORT: A CASE STUDY FROM THE GODAVARI RIVER, INDIA

by

H. M. Zwart

a MSc thesis for the Master's programme Earth, Life and Climate

Supervision:

Dr. ir. Francien Peterse – F.Peterse@uu.nl

Frédériqe M.S.A. Kirkels, MSc. – F.M.S.A.Kirkels@uu.nl

Final version

August, 2017

Course code GEO4-1520
45 ECTS

Utrecht University

ABSTRACT

The fate of SOC upon entering a river has remained largely unknown. Whereas conventional global carbon cycle models often regard river transport as a passive channel, several studies have emphasized that OC oxidation may play an important role during transport. To understand more about the properties of SOC that is discharged into the ocean and is available for carbon sequestration, it is vital to determine its provenance. For tracing SOC through a river catchment, the relative distribution of SOC-specific membrane lipids (brGDGTs) was previously employed. However, when in situ aquatic production of these brGDGTs occurs in the water column (i.e. during transport), it has proven to potentially supress the original soil-derived brGDGT signal. The recently described 6-methyl brGDGT isomers were primarily associated with primary production in a Siberian river system and may aid in identifying primary production on basis of brGDGT distribution. This study aimed to segregate these two brGDGT signals to improve the determination of the provenance of SOC that is finally discharged. Secondary goals were to evaluate the effect of increased precipitation on SOC transport and its provenance, and produce a dataset showing regional variation of bulk soil properties and brGDGT distributions throughout a catchment.

In this study, I have investigated the faith of SOC during transport in the monsoon driven Godavari River system. The geographically sharply divided soil types (relatively acidic vs relatively alkaline in the eastern and western catchment area, respectively) and bimodular precipitation regime and consequent discharge mode (baseflow characterized by high primary production versus soil erosion and transport) in the catchment area made it a perfect case study to segregate the brGDGT distributions of soil and aquatic origin.

In February (dry season) and July-August (monsoon season) 2015, soil (n = 46, dry season), SPM (n = 20 and n = 49 from dry and monsoon season, respectively) and river sediment (n = 74, 37 from each season) samples were collected in the Godavari catchment area. Physical properties

were determined and reported for Godavari soils (SOC, soil pH), Godavari River water at SPM and sediment sampling locations ($\delta^{18}O$, $\delta^{2}H$, temperature, pH, EC, sediment loading) and Godavari River sediment (TOC, pH, surface area). All samples (soil, SPM and river sediment) were freeze dried, homogenized, extracted, and then analysed for GDGTs, using an UHPLC – APCI – MS system, following method described by Hopmans et al. (2016).

Results showed that SOC transported is severely limited during the dry season: sediment loading is very low and the relative brGDGT distribution in SPM differed substantially from that of soil samples, throughout the catchment. While all samples were generally dominated by the tetramethylated brGDGT Ia, the dry season SPM samples were characterized by an increase in abundance of 6-Me isomers of penta- and hexamethylated brGDGTs.

During the monsoon season, the sediment loading of the Godavari River discharge increased exponentially. SOC erosion and transported occurred preferentially at the eastern side of the catchment area, as inferred from its sediment loading and the strong match between SPM and soil brGDGT distribution patterns, which were both characterized by a high abundance of brGDGT Ia. However, the western side of the catchment showed a brGDGT distribution pattern characterized by the 6-Me penta-and hexamethylated brGDGTs, similar as during the dry season, and seemed not to contribute to the final SOC discharge in the Godavari Delta.

Although brGDGTs can adequately be employed to trace SOC through a catchment, the processes affecting their fate during transport need further investigation before their distribution can be effectively and accurately applied in paleo-environmental reconstructions, as without a reference on the provenance of SOC it remains impossible to segregate the soil-derived brGDGT signal from transformations during transport.

Table of contents

ABSTRACT 2
1 Introduction 6
1.1 The role of soil organic matter in the global carbon cycle 6
1.2 Development of GDGT- based (paleo)environmental proxies 7
1.2.1 Microbial membrane lipids 7
1.2.2 Branched GDGTs 8
1.3 Use of brGDGTs in environmental studies and potential pitfalls 12
1.3.1 Previous application of brGDGTs 12
1.3.2 Employing brGDGTs as a soil organic carbon tracer 14
1.4 Aim 15
2 Study Area: the Godavari basin 17
2.1 The Indian monsoon 17
2.2 Geology and soil development 20
2.3 Reservoirs and dams 20
2.4 Sub-regions in the Godavari catchment 21
3 Methods and Materials 22
3.1 Field sampling 22
3.2 Sample preparation and processing 23
3.3 Environmental parameters and geochemical analysis 25
3.3.1 River water characteristics 25
3.3.2 Soil pH 25
3.3.3 TOC and TN 25
3.3.4 Carbon isotope analyses 26
3.3.5 Water isotope analysis 26
3.3.6 Surface area analysis 26
3.4 GDGT analysis 26
3.4.1 Lipid extraction and separation 26
3.4.2 GDGT analysis 28
3.4.3 GDGT-based proxy calculations 29
3.5 Data processing and statistical analysis 32
4 Results and interpretation 33
4.1 Environmental parameters and geochemical river water analysis 33
4.1.1 Hydrogen (δD) and oxygen isotopes ($\delta^{18}O$) 33

4.1.2 Sediment loading 35
4.1.3 Water temperature, pH and soil pH 35
4.1.4 Soil and river sediment organic carbon 39
4.2 Abundance of brGDGTs and isoGDGTs 44
4.3 GDGT based proxies 46
4.4 Distribution of brGDGTs 57
4.5 Numerical statistical analysis 60
4.5.1 Soils 63
4.5.2 SPM 63
4.5.3 River sediment 68
5 Discussion 69
5.1 Land-sea transport of SOC 69
5.2 Role of aquatic brGDGT production 72
5.3 Use of brGDGTs in paleoclimate reconstructions 72
6 Conclusions 73
References 75
7 Supplements 80
7.1 Digital data 80
7.2 Maps 80

1 Introduction

1.1 The role of soil organic matter in the global carbon cycle

The International Panel on Climate Change (IPCC) foresees surface air temperature increases of up to 5 °C and increased frequency of heavy precipitation events in the next century (IPCC report, 2015), mainly resulting from anthropogenically enhanced concentrations of greenhouse gases such as carbon dioxide (CO_2) and methane (CH_4). Although abrupt CO_2 variations have occurred before in the Earth's past (for example, during the hyperthermals observed in the Paleocene-Eocene (Zachos et al., 2001)), it remains unclear whether the climate system can recover from the increasing CO_2 emissions since the industrial revolution and if at all, on what timescales. To answer these questions, it is essential to develop a thorough understanding of the carbon cycle and the processes that play a role in natural pathways of carbon sequestration.

One of the most significant pathways of carbon sequestration and long-term storage of organic carbon (OC) is through burial in marine environments (Dean et al., 1998). Soil organic carbon (SOC) plays a particularly import role as it is the largest terrestrial organic carbon pool and is continuously mobilized through erosion. Rivers are key players in this process, as they provide a transport pathway of terrestrial OC from land to the oceans. In conventional global carbon models (e.g. Sarmiento and Gruber, 2002) the pathway of SOC transport to the ocean is regarded as a passive channel, whereas several studies (e.g. Cole et al., 2007; Aufdenkampe et al., 2011; Regnier et al., 2013) have estimated that only 30% of eroded SOC reaches the ocean, and that both inland storage and OC oxidation during river transport play a major role in the fate of SOC during transport. Moreover, it remains largely unknown what processes contribute to the fate of SOC during transport and at what time scales they operate. To understand more about the properties of SOC that is discharged to the ocean, it is vital to determine its provenance. Therefore, it is essential that our understanding of the dynamics of SOC land-sea transport by rivers, and the potential influences of climate change on this process, is improved.

To study the passage of SOC through the catchment and its provenance, we need a specific tracer for this carbon pool. Previous studies on the fate of soil organic carbon were based on bulk OC properties (e.g. Galy et al., 2008; Kusch et al., 2010) or plant based biomarkers (e.g. Jaffé et al., 2001; Mead et al., 2005). However, a more promising candidate is a soil-specific set of microbial membrane lipids, the branched glycerol dialkyl glycerol tetraethers (brGDGTs).

1.2 Development of GDGT- based (paleo)environmental proxies

1.2.1 Microbial membrane lipids

Whereas all eukaryotic organisms use a phospholipid bilayer as separating or enclosing membrane for their cells, some archaea employ monolayer glycerol dialkyl glycerol tetraethers (GDGTs) as cell barrier. Rather than the straight chained carbon skeletons that are found in eukaryotic lipids, the core carbon skeleton of GDGTs consists of two biphytane chains (a C_{40} isoprenoid unit) and is connected to two glycerol units with ether bonds at both terminal positions. In the natural environment, these isoprenoid GDGTs (isoGDGTs) are found with 0-8 cyclopentane moieties (DeRosa et al., 1988) in their core structure (named GDGT-0 to GDGT-8), although most common isoGDGTs are GDGT-0 to GDGT-4 (relevant chemical structures in ***Figure 1***). Crenarchaeol (or GDGT-4) has 4 cyclopentane moieties and one cyclohexane moiety.

The internal cyclization of the biphytane chains is thought to be a function of membrane fluidity moderation (Peters et al., 2005). These adaptions were commonly thought to be the result of extreme environmental stress and thought of as a mechanism to allow high temperature (>40 °C) cell growth. However, more recent studies have shown that non-extremophilic archaea are found in a wide range of environments. Moreover, the GDGT-synthesizing mesophilic Thaumarchaeota (formerly known as Crenarchaeota) are ubiquitous in lacustrine and marine environments and make up a large part of the microbial community (Schouten et al., 2013 and references therein).

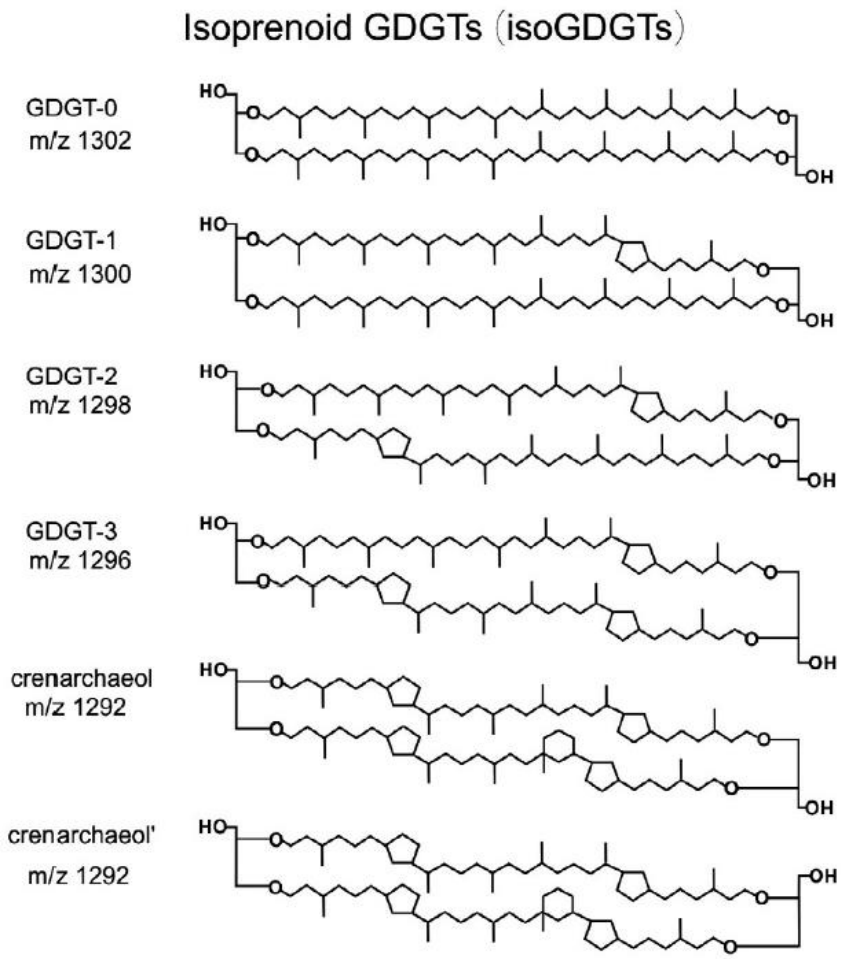

Figure 1 Isoprenoid GDGT structures and their mass to charge ratio (m/z). Note that crenarcheol' is the regioisomer of crenarcheol

1.2.2 Branched GDGTs

More recently, a structurally related compound was ubiquitously found in soils and peats (Sinnighe Damsté, 2000; Weijers et al., 2006a). Instead of an isoprenoid carbon core structure, these so called branched GDGTs (brGDGTs) were found to have two 13, 16-di- (brGDGT I) or 5, 13, 16-trimethylated ('branched') octacosane (brGDGT III) skeletons, or a combination of both (brGDGT II). Weijers et al. (2006b) identified additional brGDGTs containing cyclopentane moieties (all relevant brGDGT molecular structures in **Figure 2**). Although their origin is still unknown, the stereochemistry of the glycerol backbone suggests a bacterial or eukaryotic source (Schouten et al., 2013 and sources therein).

The relative distribution of different brGDGTs in a soil depends on mean annual temperature (MAT) and soil pH: Weijers et al. (2007) found that the number of methylations on the alkyl chains increases with decreasing temperature and that brGDGTs containing more cyclopentane moieties prevail in more alkaline soils. To quantify these changes in distribution, the methylation of branched tetraethers (MBT) and cyclization of branched tetraethers (CBT) indices were defined (Weijers et al, 2007). After studying an extended global soil dataset which showed a significant correlation with only seven out of nine brGDGTs, Peterse et al. (2012) simplified the MBT-index by removing two minor components (brGDGT IIIb and IIIc) and the MBT-index was redefined as MBT'. However, the new transfer function for the extended dataset showed a substantially lower correlation with MAT (r^2 = 0.58, n=278) than the original (r^2 = 0.78, n=176). Precipitation seemed to be an important factor in this lower correlation coefficient, as soils from arid regions (MAP<500mm) could be underestimated in temperature by up to 20°C (Peterse et al., 2012). Several studies on the effect of soil water content (SWC) on the distribution of brGDGTs have shown that the CBT-MBT'-index does not always produce reliable temperatures in arid and semi-arid regions (MAP < 700-800 mm year^{-1}; Dirghangi et al., 2013), and MBT is primarily driven by water availability in these regions, rather than MAT (Menges et al., 2014). Recently, De Jonge et al. (2013) discovered a new set of brGDGT isomers. This set of brGDGT isomers differs in the position of the methyl groups on the carbon skeleton. Rather than at the 5 or 5'-position, the methyl groups of these brGDGTs are positioned at the 6 or 6' position (Figure 2). De Jonge et al. (2014a) find that the abundance of the '6-methylated' (6-Me) brGDGTs strongly correlates with pH and that the MBT'$_{5ME}$ (the 6-Me brGDGTs are excluded from this index) is no longer dependant on soil pH, but rather only on MAT. Therefore, they conclude that the separate quantification of 5- and 6-Me brGDGTs is essential for accurately reconstructing environmental parameters based on relative distributions of brGDGTs. A recently published improved chromatographic methodology (Hopmans, et al., 2016) allows the separate quantification of these isomers.

Soil pH and SWC generally co-vary and consequently, pinpointing the one controlling 6-Me brGDGT distribution is difficult (i.e., a correlation between pH and brGDGTs could in fact be a correlation with varying SWC, while pH mimics SWC variation). Therefore, along a SWC transect with relatively constant soil pH, Dang et al. (2016) studied the effect of water availability on the relative contribution of 5- and 6-Me brGDGTs. They found that soil water content may control the degree of methylation on 6-Me brGDGTs, while 5-Me brGDGTs are more influenced by temperature. They suggested that when the abundance of 6-Me brGDGTs exceeds 50%, brGDGT-based paleothermometers become inaccurate and their variation results from MAP, rather than from temperature.

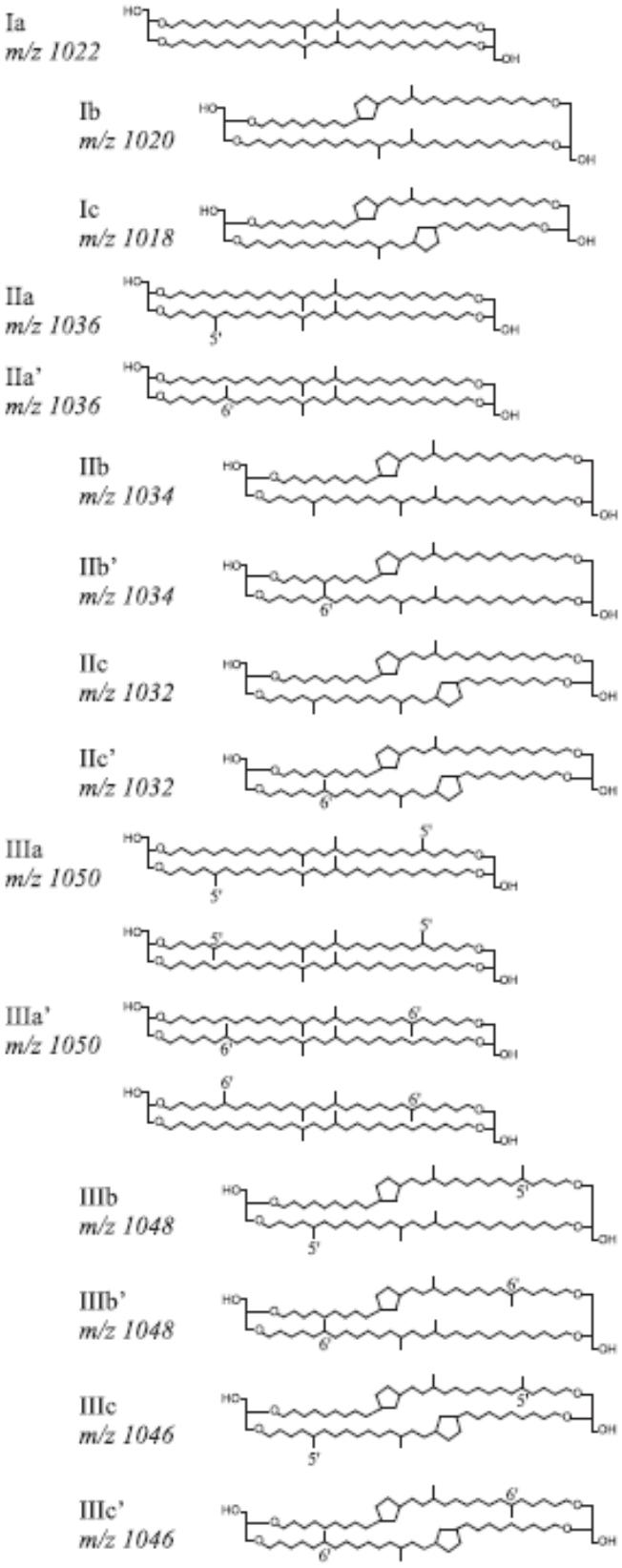

Figure 2 Branched GDGT (brGDGT) structures. Note the '-marked brGDGTs are isomers that have a methyl-group at the 6- or 6'-position rather than the 5- or 5'-position.

1.3 Use of brGDGTs in environmental studies and potential pitfalls

1.3.1 Previous application of brGDGTs

The brGDGT signal from soils is transported from land to sea by rivers, through erosion. Therefore, hypothetically, the brGDGT signal that is found in marine coastal regions (SPM and sediments) should reflect the signal found in upstream soils and give insight in the governing physical conditions (i.e., temperature and pH) of the source area. In addition, the relative abundance of brGDGTs compared to that of the isoGDGT crenarchaeol, can give insight in the relative input of terrestrial OC into a marine setting. Crenarchaeol typically dominates over brGDGTs in marine environments, although also found in aquatic environments (Hopmans et al., 2004; Weijers et al., 2006b). That these two end-members are both characteristic for a typical environment aids in determining the contribution of each to the carbon pool. So, principally, brGDGTs are typical for the soil carbon end-member, whereas crenarchaeol is typical for the marine carbon end-member (also see ***Figure 3***). The ratio of brGDGTs and crenarchaeol then gives an impression of the terrestrial contribution to the total pool of OC (defined as the branched and isoprenoid tetraether (BIT) index, see 3.4.3, equation 1). However, the assumption that the origin of these two end-members is exclusive (soil for brGDGTs and marine for crenarchaeol, respectively) seems to be debaTable (see next section on aquatic brGDGT production and discussion on occurrence of crenarchaeol in soils in Weijers et al., 2006a and Schouten et al. 2012) and this complicates the utility of the BIT index.

In paleo-climate reconstructions, these principles have been applied and downcore variations in coastal marine sediments have been shown to give insight in ancient conditions (e.g. Weijers et al, 2007).

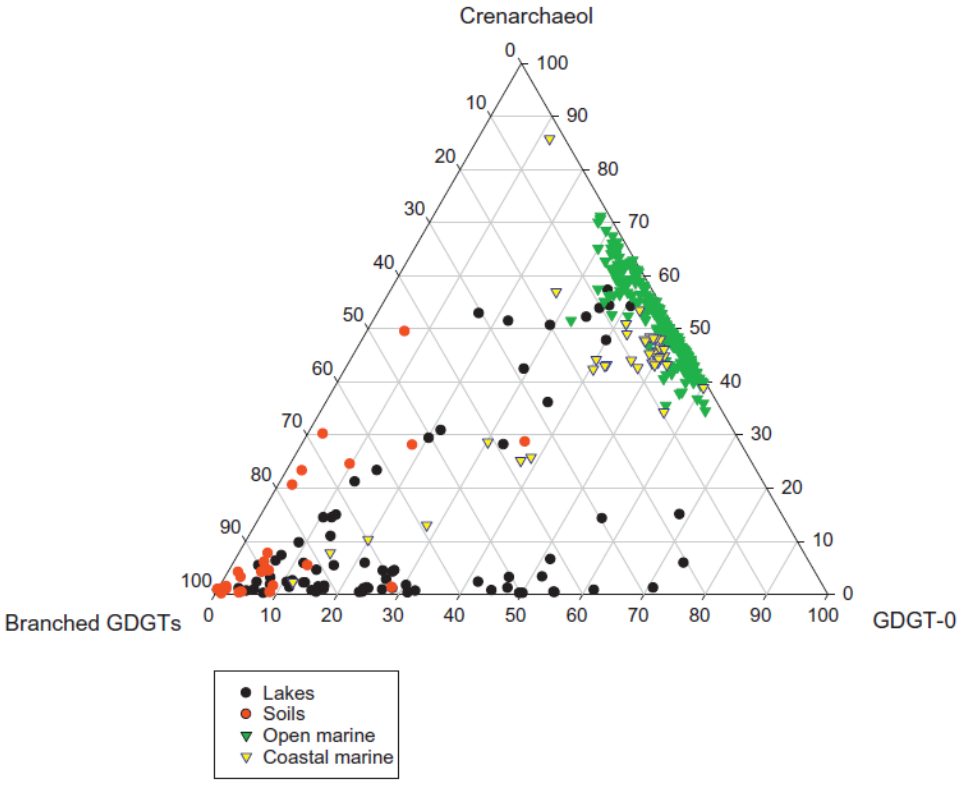

Figure 3 Ternary diagram of the contribution of brGDGTs, GDGT-0 and Crenarchaeol in modern environment organic carbon. *After Schouten, et al. (2013).*

Whereas the global MAT and pH calibration showed a lot of potential, early complications included erroneous reconstruction of temperature variation with source area changes (Schouten et al., 2008; Donders et al., 2009, Bendle et al., 2010) and in lake settings (e.g. Tierney et al., 2012; Wang et al., 2012). For example, the trend in the brGDGT based temperature record from the Amazon River fan covering the Last Glacial Maximum appeared reversed. Rather than showing a decreasing temperature, it seemed to increase, which Bendle et al. (2010) attributed to the soil organic matter provenance changing from the high Andes (lower temperatures) to the flood plains (higher temperatures).

In addition, an underestimation of temperatures in lake settings was found (e.g. Tierney et al., 2012; Wang et al., 2012) which was thought to be an artefact of potential *in situ* aquatic production. *In situ* production of brGDGTs in the water column would also severely complicate tracing a soil signal throughout a catchment area.

1.3.2 Employing brGDGTs as a soil organic carbon tracer

The ubiquitous presence of brGDGTs in globally distributed soils (Weijers et al., 2006a) led to the presumption that brGDGTs find their origin in soils. This is the key characteristic of brGDGTs that would make them a suiTable SOC-specific tracer. Their distribution can subsequently be used to trace the provenance of the soil OC. However, only when the different parts of a catchment have a distinct brGDGT signature. This has already been applied in a study on the origin of brGDGTs in the Amazon River (Zell et al., 2013a), who compared the brGDGT distributions in organic matter between soil and SPM. However, they found a mismatch between the brGDGT distribution in Amazon lowland soils and the brGDGT distribution found in Amazon SPM. Furthermore, they revealed the presence of intact polar lipid (IPL)-derived brGDGTs in the water column, in higher concentrations than found in the soil organic matter. They contributed this mismatch in brGDGT signal and enrichment in IPL-derived brGDGTs to *in situ* aquatic production of brGDGTs in the Amazon River. If production of brGDGTs takes place during river transport, this can severely alter the initial distribution of brGDGTs in soils during transport, a potential pitfall in the application of brGDGTs as a SOC specific tracer.

Other river systems that have previously been investigated for brGDGTs are the Têt River (Kim et al., 2011), the Amazon River (Zell et al., 2013a, 2013b, 2014a), the Yenisei River (De Jonge et al., 2014b), the Tagus River (Zell et al., 2014b), the Yangtze River (Li et al., 2015), Madre de Dios (Kirkels, *in prep.*), the Colville River (Hanna et al., 2016), and the Danube River (Freymond et al, 2017). From these studies, we learned that the provenance of eroded soil organic matter can be traced by comparing the relative distribution of brGDGTs in river SPM to that of soil organic matter in the catchment area. Although, the most recent studies on brGDGT derived SOC transport through a river catchment suggest that the transported brGDGT signal is mostly a local signal (e.g. Kim et al., 2015; Freymond et al., 2017). This would imply that the signal

transported to river deltas and into marine sediment is not representative for upstream conditions, but rather records the local environment.

Also, it became clear that the brGDGT distribution can be altered during transport as a result from aquatic production of brGDGTs. The most pertinent question that remains before the provenance of soil organic matter can be determined using brGDGT distributions, is how can we can segregate the 'original' soil brGDGT signal from a possible modification by aquatic production during transport.

To get closer to answering this question, ideally, a river system is required where soil erosion and subsequent river transport, and a baseflow system characterized by high primary production are naturally segregated, either in space or time. This way their respective brGDGT signals could be studied separately without interference.

1.4 Aim

In this study, I will investigate the fate of SOC during river transport from the Godavari basin to the Bay of Bengal, the second largest river system in India after the Ganges-Brahmaputra (see section 2 for detailed study area information). The high difference in precipitation between the monsoon season and dry season and resulting fluctuations in river discharge should allow for comparing the baseflow (i.e. the OC signal associated with low-water discharge and during dry season) and peak flow OC (i.e. the OC signal that is supplemented with surface run-off and associated soil erosion) discharge. Also, the natural west-east gradient in precipitation and vegetation that is present in the Godavari catchment area should further enable to study the provenance of SOC. Finally, the monsoon-driven precipitation regime makes the Godavari River system a highly suiTable analogue, to study the effects of the projected increases in precipitation for the future on SOC transport.

The main objectives of this study are to 1) assess the provenance and quantity of SOC finally discharged by the Godavari River, by comparing the Godavari delta biomarker and SOC signatures in river suspended particulate matter (SPM) during dry and monsoon seasons to the OC signal in a selection of upstream river bed sediments and catchment soils, and 2) assess the effect of increased precipitation on the provenance and quantity of river-transported SOC, by comparing the biomarker and SOC signatures in SPM between the dry and monsoon season (i.e. February-March vs July-August 2015). Secondary objectives are to compile high resolution maps of bulk soil properties and brGDGT distributions throughout the catchment.

2 Study Area: the Godavari basin

2.1 The Indian monsoon

With an average discharge of 3,505 $m^3 s^{-1}$ and a catchment area of over 300,000 km^2 the Godavari River is the second largest river in India, after the Ganges-Brahmaputra system. The discharge of the Godavari River is primarily driven by precipitation and is distributed highly disproportionally over the year. The precipitation between June and September provides for roughly 85% of the mean annual precipitation (MAP, ***Figure 4***). The sediment load of the Godavari River is equally skewed towards the monsoon season (Rao et al., 2015) and almost no transport takes place during the dry season. This is the result of seasonally heavy rainfalls associated with the arrival of the Indian monsoon during boreal summer.

Principally this phenomenon is the result of a differential in heating of land and sea masses. The Indian subcontinent warms quicker than the surrounding Indian Ocean, which results in a large-scale surface temperature gradient. This gradient is accompanied by a pressure difference and consequently induces a land inward surface flow of humid air. In the Godavari catchment, the annual precipitation regime (***Figure 4***) is characterized by an east-west decreasing trend, where the north-eastern region receives almost a five-fold in precipitation compared to the dry western region. Whereas most of this difference is exhibited during the monsoon season, also during the rest of the year the western area generally receives less precipitation.

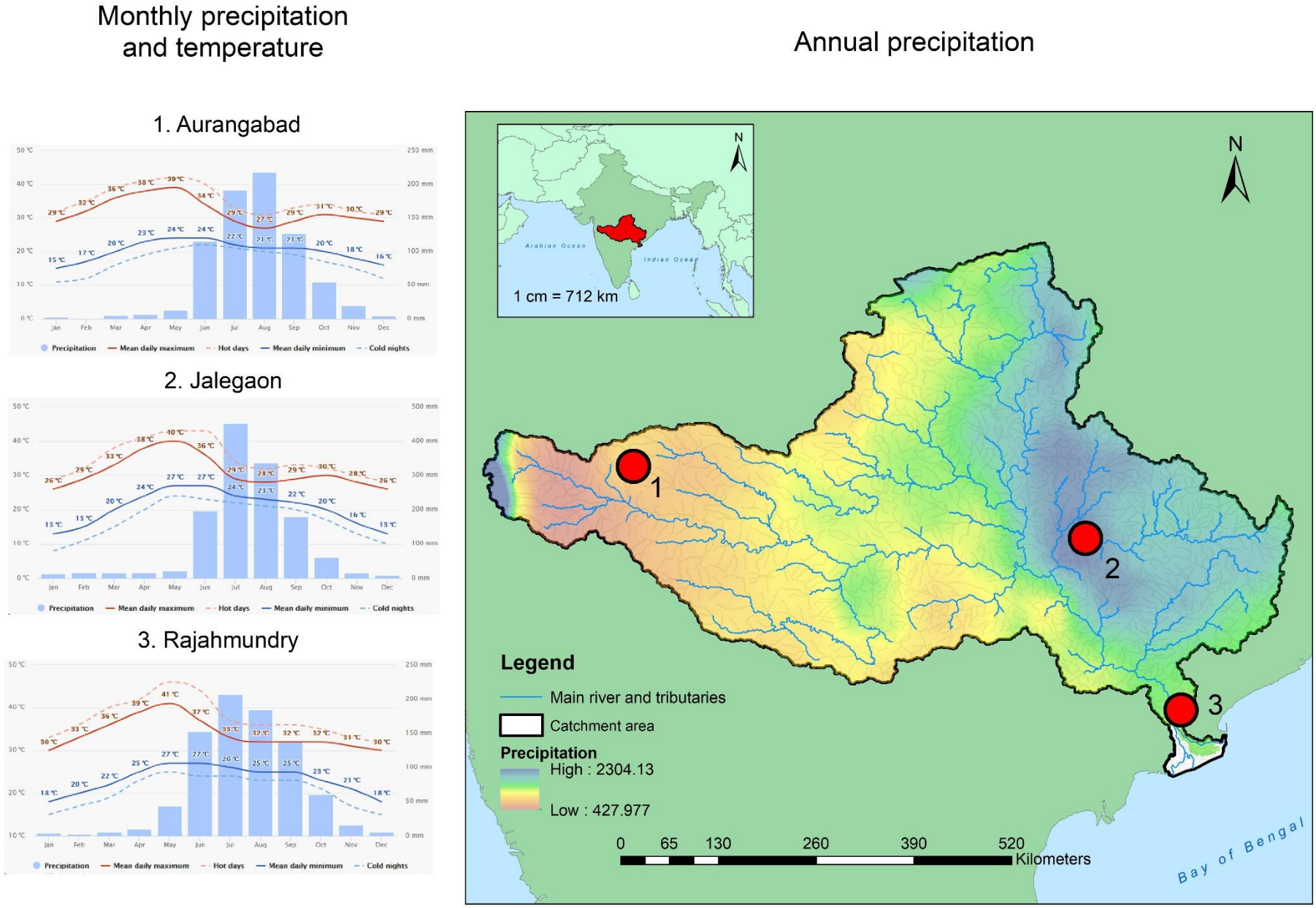

Figure 4 The Godavari catchment area, showing the Godavari River and its main tributaries and mean annual precipitation (MAP) based on APHRODITE (Asian Precipitation - Highly-Resolved Observational Data Integration Towards Evaluation). For three locations, the monthly distribution of precipitation and air temperature has been specified (**note:** the scaling on the precipitation axis (right-side) is different)

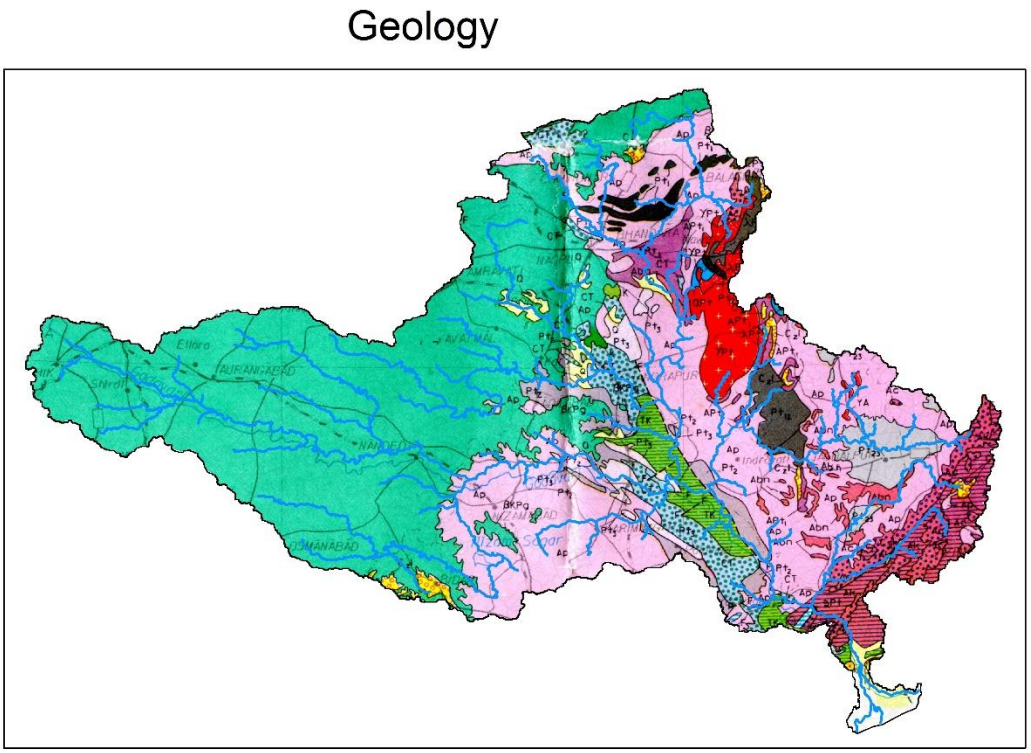

Figure 5 Geological map of the Godavari area. Pink areas represent the Indian shield lithologies, consisting of Archean shales and gneisses, whereas greenish areas represent Deccan Trap lithologies (large igneous provinces associated with large scale volcanism, which initiated during the Late Cretaceous).

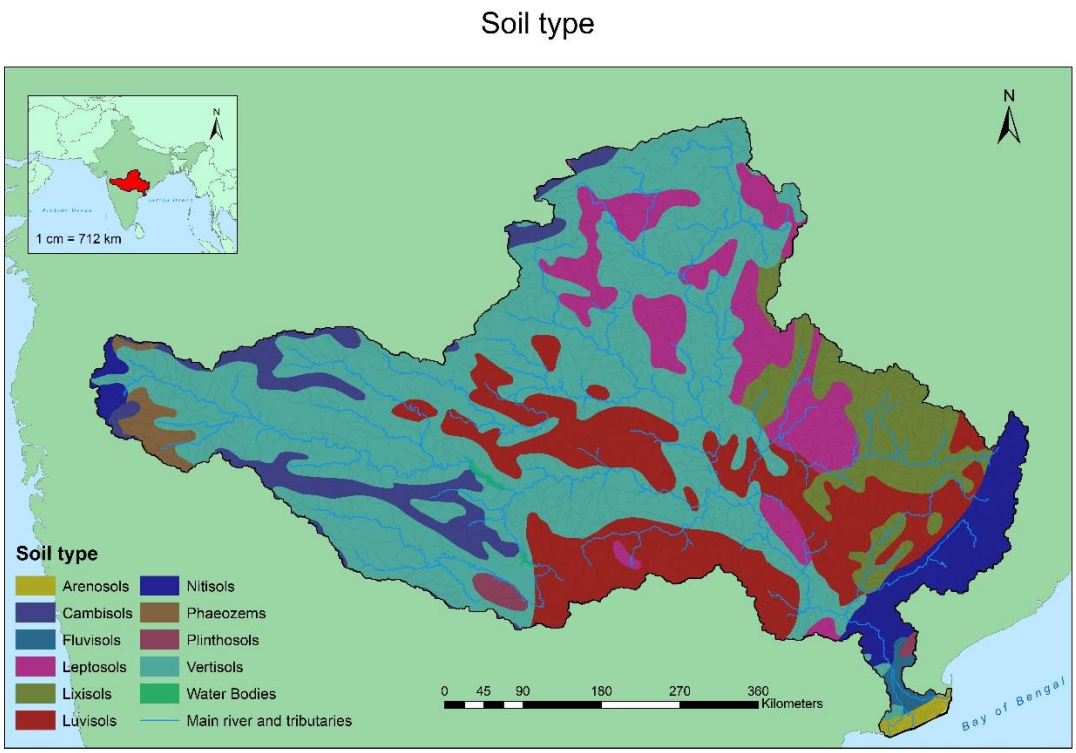

Figure 6 Soil type in the Godavari catchment area, overlain with the Godavari river and its main tributaries. From Harmonized World Soil Database (*HWSD), version 1.1., Food and Agriculture Organization of the United Nations (FAO) and the International Institute for Applied Systems Analysis (IIASA) combined effort soil map,* 2009

2.2 Geology and soil development

The surface geology in the Godavari catchment (***Figure 5***) is sharply divided into a western and eastern region with each having a distinctly different predominant lithology. In the eastern area, these are predominantly Archean gneisses and schists, while in the western area these are predominantly flood basalts originating from the Deccan Traps. Weathering of this bedrock forms clayey and loamy material that is prone to erosion. The soil development in these areas are equally different: soils overlaying the western basalts are predominantly more alkaline vertisols (USDA soil taxonomy), whereas eastern soils, overlaying the Archean gneisses and schists are typically acidic and poorly developed alfisols (Ray et al., 1997).

2.3 Reservoirs and dams

Apart from its religious significance, the Godavari River is also an important contributor to successful agriculture and energy production. The many dams along the course of the main river and its tributaries ensure the possibility of irrigation and production of electricity through hydropower. The amount of these structures severely limits the natural flow throughout the catchment area. The area where natural flow is limited by human-made structures almost spans half of the catchment area (see the checked area in ***Figure 7***).

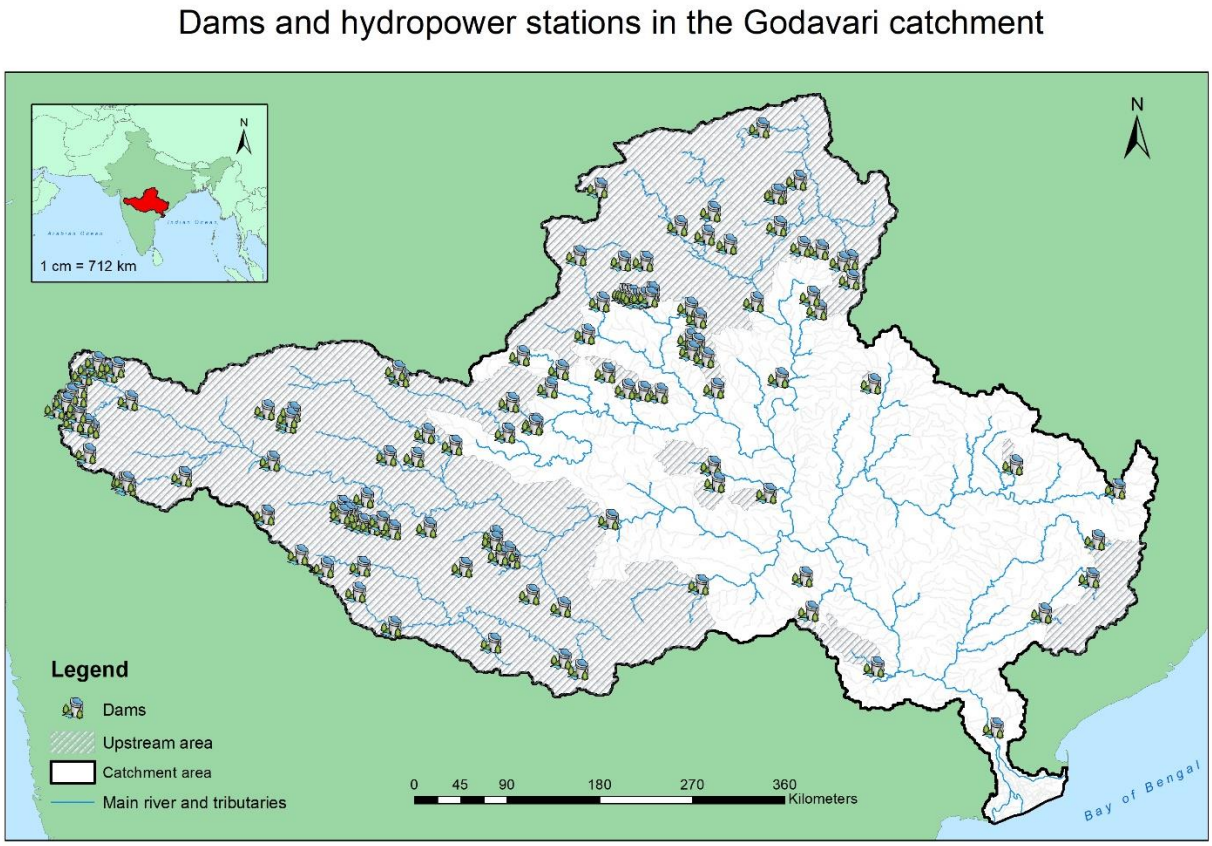

Figure 7 The locations of different dams and hydropower stations. The displayed locations were manually pin-pointed from satellite images. The area of the catchment that has a dam located downstream is shaded (note: the major Dowleswaram Barrage at Rajahmundry in the Godavari delta has knowingly been left out – principally the entire catchment area is 'dammed')

2.4 Sub-regions in the Godavari catchment

The irregular spatial distribution in precipitation, geology and soils between different areas in the Godavari catchment show that observed catchment-wide phenomena may not be representative for local areas, and vice versa. Therefore, to carefully study regional effects, the Godavari basin was subdivided in regions, based on its main tributaries (***Figure 8***). These are: The Upper Godavari (major tributaries are the Pravara, Purna, Manjira and Manair) and PWW regions (Pranhita, Wainganga and Wardha tributaries) which confluence with part of the IS region (Indrivati and Sabari tributaries) to the Middle Godavari. The final regions, further downstream, are the Dowleswaram Reservoir and Godavari Delta region. The Godavari Delta region comprises of the area between the reservoir and the Bay of Bengal.

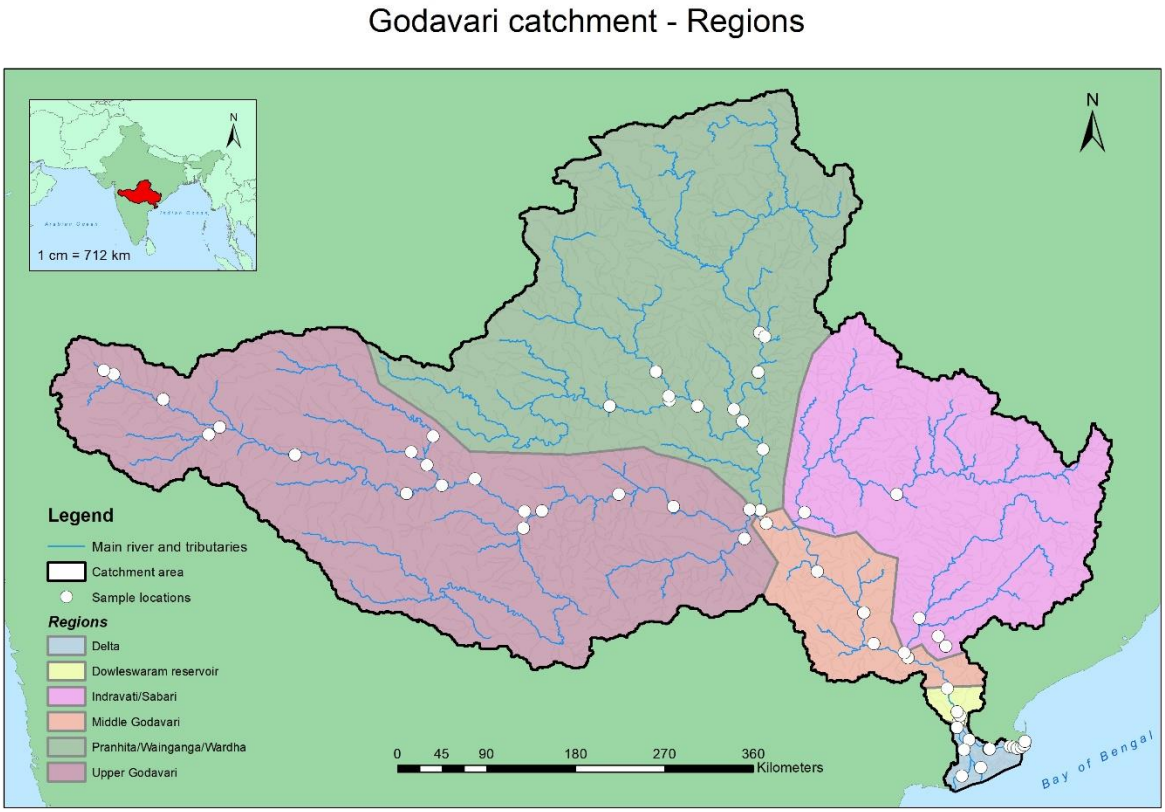

Figure 8 Godavari catchment sub-regions as used further in this study. See text for details.

3 Methods and Materials

3.1 Field sampling

Along the stretch of the Godavari river and a selection of its tributaries, samples were collected during two separate field campaigns in February (i.e. the dry season) and July-August (i.e. the monsoon season) 2015, respectively. During both campaigns, river water and river sediment were sampled, whereas soil samples were taken only during the dry season campaign.

The river water for suspended particulate matter (SPM) and sTable isotope (oxygen, hydrogen) analysis was obtained from mid-channel, where accessible (i.e. when a bridge was a present), using a plastic bucket and transferred to pre-rinsed plastic containers for transport. When the mid-channel was inaccessible, the water sample was taken as close to mid-channel position as possible, from the side. This is procedure was also employed for river sediment samples: when

the mid-channel position was accessible, these were taken using a Van Veen sediment grab (Eijkelkamp). Otherwise, they were taken from the river bank using a pre-rinsed shovel. Soil samples were also collected with a pre-rinsed shovel. Whereas a fraction of each soil sample was sieved at Utrecht University after freeze drying (63 μm sieve), the river sediment samples were sieved on site. All samples were stored in open-top polythene geological sampling bags and these were closed using duct tape prior to transport.

River water for isotope analysis was passed over a 0.45 μm cellulose acetate filter. To obtain the SPM from the river water approximately 10-50 L of river water was filtered over pre-combusted (450 °C, 6h) 0.7 μm glass fibre filters (GF/F, Whatman, Maidstone, United Kingdom) using pressurized steel filtration units (the device used and described by Lupker et al., 2011), within 12 hours of sampling. The filters were then folded in pre-combusted aluminium foil and kept cool (cf. 4 °C) during further transport. Upon arrival at Utrecht University (1-5 weeks later) all samples were stored frozen at -40 °C. At two sites (W 10 and W28, and G 10, for monsoon and dry season campaigns, respectively) depth profiles were taken using a custom-built horizontally orientated water sampler (the device used is described in Galy et al., 2007; Galy and Eglinton, 2011).

3.2 Sample preparation and processing

Prior to further processing, all GF/F filters with SPM, river sediment (bulk and < 63 μm fraction) and soil samples were freeze-dried. The bulk soils and sediments were then homogenized using a planetary ball mill (PM 400, Retsch GmbH, Haan, Germany) with stainless steel buckets and balls, an agate ball mill (Pulverisette 6 centrifugal ball mill, Fritsch GmbH, Idar-Oberstein, Germany) or manually using an agate mortar and pestle. Small contaminants such as pebbles, rootlets or plant tissue were manually removed prior to homogenisation. The handling materials were thoroughly rinsed with water and acetone between samples to prevent cross-contamination.

Sample locations

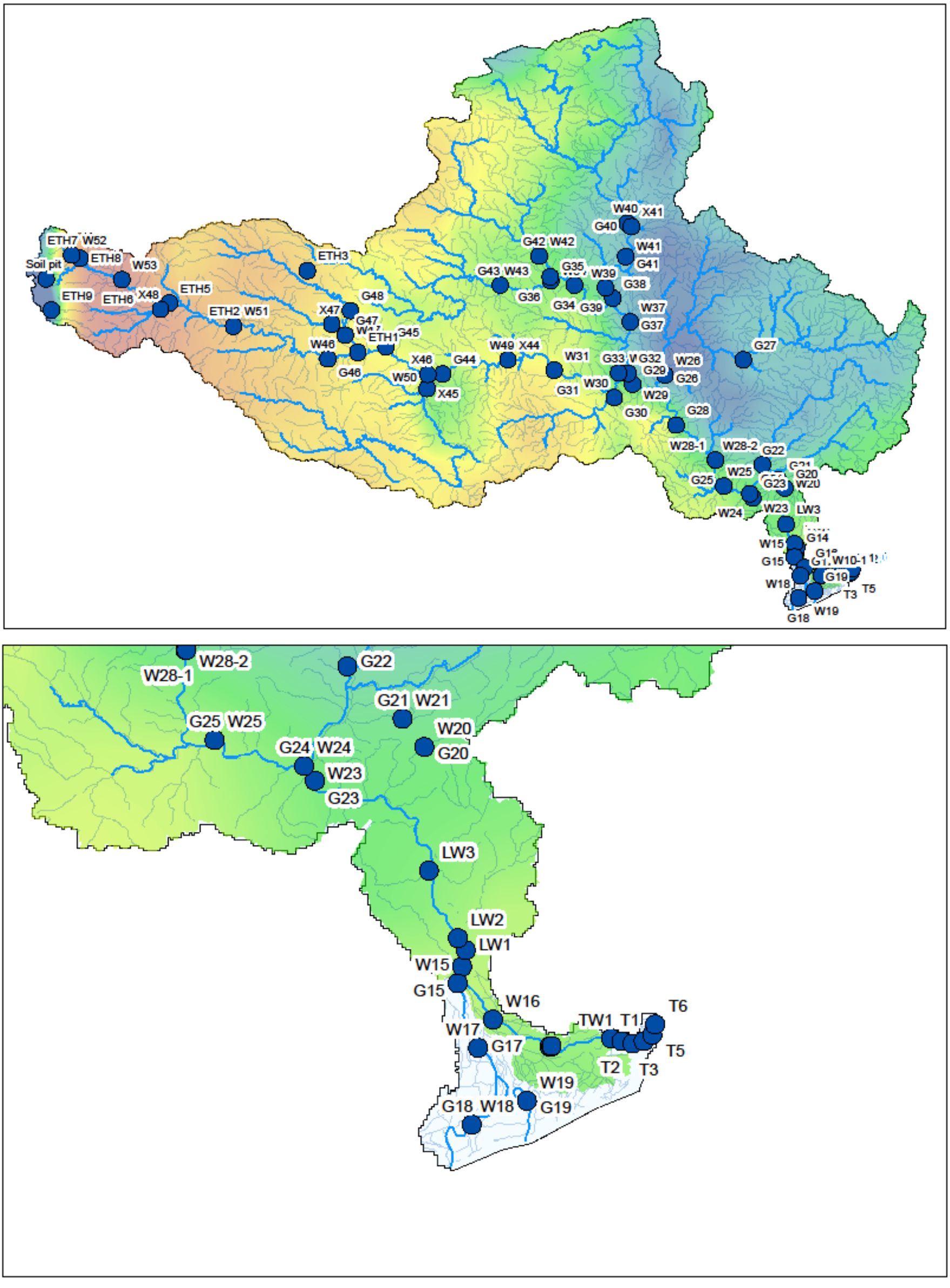

Figure 9 Sampling locations of this study. Samples numbered with 'W' are from the monsoon season sampling campaign, whereas all others are from the dry season campaign.

3.3 Environmental parameters and geochemical analysis

3.3.1 River water characteristics

Physical and chemical characteristics of river water were measured in situ. Water temperature, electrical conductivity and oxygen saturation were measured using a Hach HQ30d and HQ40d multi-parameter meter fitted with a IntelliCAL PHC101 pH gel-filled probe, CDC401 conductivity probe and LDO101 luminescent/optical dissolved O2 probe. The pH and EC probes were calibrated on a biweekly basis using Singlet buffer solutions with pH 4.01 and 7.00 (Hach-Lange) and 1, 0.1 and 0.01 M KCl, respectively.

3.3.2 Soil pH

The pH of soils and sediments were measured in Utrecht in a 1:5 (v:v) sample (freeze-dried) to distilled water mixture. The mixture was shaken for 30 min at 200 RPM and left to settle overnight at 4°C. The pH was measured with a SympHony SB70D meter and 14002-850 pH electrode, calibrated with CertiPUR buffer solutions with pH 4.01, 7.00 and 10.00.

3.3.3 TOC and TN

The Total Organic Carbon (TOC) and Total Nitrogen (TN) content of soils and river sediments (bulk only) were analysed with an Elemental Analyser at Utrecht University. Prior to analysis, glassware and silver capsules were combusted at 450°C for 6h to remove OC traces. Sample preparation further consisted of decarbonation by acid vaporization treatment: samples were placed in a desiccator with approximately 100 mL concentrated HCl 37% at70 °C for at least 72h, as described by Komada et al. (2008) and Van der Voort et al. (2016). Subsequently, the samples were dried at 70 °C, with sodium hydroxide (NaOH) pellets added inside the desiccator for removal of the acidic fume.

3.3.4 Carbon isotope analyses

The radiogenic ($\Delta^{14}C$) and sTable ($\delta^{13}C$) carbon isotope compositions of soil were measured by Usman (in prep.) on a MI-CADAS (MIniturised radioCArbon DAting System) at the Laboratory of Ion Beam Physics, ETH Zürich (procedures described by Wacker et al., 2010).

3.3.5 Water isotope analysis

Hydrogen and oxygen isotopes of river water were analysed by Kirkels (in prep.) using a LGR 912 Off-Axis Integrated Cavity Output Spectrometer (OA-ICOS) at NIOZ (Texel, The Netherlands). Values are reported relative to the VSMOW standard (Gonfiantini, 1978) in delta notation (i.e. $\delta^{16}O$ and $\delta^{2}H$, i.e. δD).

3.3.6 Surface area analysis

A number of river sediment samples was selected for surface area analysis. The surface area measurements were carried out using a BET multi-point nitrogen physisorption apparatus (Micromeritics Tristar II 3020) at ETH Zürich. The nitrogen adsorption was measured from an eleven-points isotherm in a relative pressure P/P0 range of 0.05 to 0.30 at 77.3 K. The freeze-dried samples were degassed using an external degassing station (VacPrep 061 from Micromeritics), under vacuum and N_2 flow for at least 3 hours.

3.4 GDGT analysis

3.4.1 Lipid extraction and separation

Soil and sediments (bulk and < 63 μm fraction) and GF/F filters containing SPM samples were extracted using an Accelerated Solvent Extractor (ASE 350, Dionex, Thermo-Scientific). The samples were extracted with a 9/1 (v/v) solvent mixture of dichloromethane (DCM)/methanol (MeOH) at 100 °C and 7.6 × 106 Pa. The obtained total lipid extract (TLE) was dried under N_2 flow and a 20% aliquot was kept separately, functioning as back-up.

The TLE of SPM from the dry season, river sediments (bulk and < 63 μm fraction) and soils < 63 μm was separated into an apolar, intermediate and polar fraction by column chromatography, using aluminium oxide (Al_2O_3) as stationary phase and hexane, a 1/1 (v/v) mixture of hexane and DCM and a 1/1 (v/v) mixture of DCM and MeOH as eluents, respectively.

Bulk soil samples, as well as SPM samples from the monsoon season, were selected for fatty acid analysis (outside the scope of this study, reported elsewhere) and consequently treated differently than the other samples. The TLE of these samples was firstly saponified with KOH (dissolved in MeOH, 0.5 M, 2h at 70°C), following the procedure described by Freymond et al. (2016). Sodium chloride-enriched milliQ water (approx. 1 tbsp. NaCl per litre) was added to enhance separation, after which the neutral fraction was back-extracted with hexane (3x 10 mL). The remaining mixture was acidified by adding 1.5M HCl (dissolved in MeOH) until the desired pH of ~2 was reached. Subsequently, by back-extraction with a 4/1 mixture (v/v) of hexane and DCM (3x 10 mL), the acid fraction was isolated for further analysis as ETH Zürich. The neutral fraction was then passed over a sodium sulphate (Na_2SO_4) column to remove any remaining water. The remaining procedure to obtain the polar and apolar fractions was similar to the procedure applied to the rest of the samples: the neutral fraction was passed over an activated Al_2O_3 column and separated into an apolar fraction and polar fraction using hexane, and a 1/1 mixture (v/v) of DCM and MeOH as eluents, respectively. All solvents were evaporated from sample vials by applying heat (30 °C) and gas (N_2)-flow. Sequentially, they were stored at approximately 6 °C before analysis.

3.4.2 GDGT analysis

The polar fraction, containing the GDGTs, was dissolved in a 99/1 mixture (v/v) of hexane and isopropanol. For quantification, a synthetic C46 GDGT standard (Huguet et al., 2006) was added, the mixture was subsequently passed through a 0.45 μm PTFE filter to remove any remaining particles prior to injection on the HPLC system.

An Ultra High Performance Liquid Chromatograph (Agilent 1260 Infinity, Agilent Technologies, Santa Clara, CA, USA) coupled to an Agilent 6130 quadrupole Mass Spectrometer (UHPLC – APCI – MS) was used, employing two silica Waters Acquity UPLC BEH Hilic columns (150 × 2.1 mm; 1.7 μm; Waters corp., Miliford, MA, USA) at 30 °C, preceded by a silica guard column, to further separate the GDGTs (following the method of Hopmans et al., 2016). Sample injection volume was set at 10 μL and flow rate at 0.2 mL/min. The sample was separated isocratically, using two solvent systems, hexane (A) and a 9/1 (v/v) mixture of hexane and isopropanol (B). For 25 minutes, the ratio was set at 82% A and 18% B. This was followed by a linear gradient analysis towards 70% A and 30% B and then to 100% B in totally 30 minutes. Each run was followed by a 20-min equilibrium phase. Conditions for APCI-MS were: nebulizer pressure 60 psi, vaporizer temperature 400 °C, drying gas (N_2) flow at 6 L/min and gas temperature 200 °C, capillary voltage −3500 V, corona 5.0 μA.

The HPLC system was operated in selected ion monitoring (SIM) mode, where detection was achieved at m/z = 1302 (GDGT-0), 1300 (GDGT-1), 1298 (GDGT-2), 1296 (GDGT-3), 1292 (GDGT-4: Crenaercheol), 1050 (brGDGT IIIa), 1048 (brGDGT IIIb), 1046 (brGDGT IIIc), 1036 (brGDGT IIa), 1034 (brGDGT IIb), 1032 (brGDGT IIc), 1022 (brGDGT Ia), 1020 (brGDGT Ib), 1018 (brGDGT Ic) and 744 (synthetic GDGT standard), and if applicable, their isomers (De Jonge et al., 2014a).

GDGT concentrations were obtained by using Agilent Chemstation B.04.03 software to calculate peak areas in the corresponding mass chromatograms. These were normalized to calculated peak area for the internal standard and corrected for sample amount prior to extraction, and the used fraction (80%) of TLE.

3.4.3 GDGT-based proxy calculations

Rather than the absolute GDGT concentrations, the fractional abundances of GDGTs are often used in GDGT-based proxies, where fractional abundance is defined as the concentration of a specific GDGT normalized by the total sum of all GDGT concentrations. The different GDGT and brGDGT abbreviations used (numerals, roman numerals, letter annotations and ') refer to their corresponding compounds or their isomers, see section 1.

Branched Isoprenoid Tetraether (BIT) index

The BIT index was calculated following Hopmans et al. (2004). The recently identified 6-methyl isomers (De Jonge et al., 2013; De Jonge et al., 2015a; De Jonge et al., 2015b) were included; producing the following final equation for calculating the relative abundances of brGDGTs and the isoprenoid GDGT crenarchaeol:

$$\text{BIT} = \frac{\text{Ia} + \text{IIa} + \text{IIIa} + \text{IIa'} + \text{IIIa'}}{\text{Ia} + \text{IIa} + \text{IIIa} + \text{IIa'} + \text{IIIa'} + \text{IV}} \quad (1)$$

Cyclization ratio of branched tetraethers (CBT') index

For reconstructing pH values, using the CBT' index, according to De Jonge et al. (2014a):

$$\text{pH} = 7.15 + 1.59 \cdot \text{CBT'} \quad (2)$$

Where the CBT' index is defined by the following equation:

$$(3) \quad \mathrm{CBT'} = log_{10}\left(\frac{\mathrm{Ic + IIa' + IIb' + IIc' + IIIa' + IIIb' + IIIc'}}{\mathrm{Ia + IIa + IIIa}}\right)$$

Reconstructed Mean Annual Air Temperature (MAT_{mr})

The reconstructed MAT was based on multiple linear regression, defined by De Jonge et al. (2014a):

$$(4) \quad \mathrm{MAT_{mr}} = 7.17 + (17.1 \cdot \mathrm{Ia}) + (25.9 \cdot \mathrm{Ib}) + (34.4 \cdot \mathrm{Ic}) - (28.6 \cdot \mathrm{IIa})$$

Isomer ratio (IR, IR_{penta}, IR_{hexa})

The isomer ratio characterizes the relative abundance of 6-methylated GDGTs (modified after De Jonge et al., 2014b; De Jonge et al., 2015a; De Jonge et al., 2015b):

$$(5) \quad \mathrm{IR} = \frac{\mathrm{IIa' + IIb' + IIc' + IIIa' + IIIb' + IIIc'}}{\mathrm{IIa + IIb + IIc + IIIa + IIIb + IIIc + IIa' + IIb' + IIc' + IIIa' + IIIb' + IIIc'}}$$

After Sinnighe Damsté (2016), this was calculated separately for penta- (IR_{penta}) and hexamethylated brGDGTs (IR_{hexa})

$$(6) \quad \mathrm{IR_{penta}} = \frac{\mathrm{IIa' + IIb' + IIc'}}{\mathrm{IIa + IIb + IIc + IIa' + IIb' + IIc'}}$$

$$(7) \quad \mathrm{IR_{hexa}} = \frac{\mathrm{IIIa' + IIIb' + IIIc'}}{\mathrm{IIIa + IIIb + IIIc + IIIa' + IIIb' + IIIc'}}$$

Isomer percentage (IP)

The abundance of the penta- and hexamethylated brGDGTs was also expressed relative to the sum of all brGDGTs, separately for 5-Me and 6-Me brGDGTs:

(8) $$IP_{5\text{-Me}} = \frac{IIa + IIb + IIc + IIIa + IIIb + IIIc}{\Sigma\ brGDGTs} \cdot 100\%$$

(9) $$IP_{6\text{-Me}} = \frac{IIa' + IIb' + IIc' + IIIa' + IIIb' + IIIc'}{\Sigma\ brGDGTs} \cdot 100\%$$

Finally, the ratio of 6-Me brGDGTs versus 5-Me brGDGTs was expressed by:

(10) $$IP_{6/5\text{-Me}} = \frac{IP_{6-Me}}{IP_{5-Me}} \cdot 100\% = \frac{IIa' + IIb' + IIc' + IIIa' + IIIb' + IIIc'}{IIa + IIb + IIc + IIIa + IIIb + IIIc} \cdot 100\%$$

Methylation and cyclisation of brGDGTs

The weighted average number of cyclopentane moieties (#Rings = number of rings) was calculated for the tetra- and penta-methylated brGDGTs, and for the latter separately for 5-Me and 6-Me penta-methylated brGDGTs, as follows (following Sinninghe Damsté, 2016):

(11) $$Rings_{tetra} = ([Ib] + 2 * [Ic]) / ([Ia] + [Ib] + [Ic])$$

(12) $$\#Rings_{penta\_5ME} = ([IIb] + 2 * [IIc]) / ([IIa] + [IIb] + [IIc])$$

(13) $$\#Rings_{penta\_6ME} = ([IIb'] + 2 * [IIc']) / ([IIa'] + [IIb'] + [IIc'])$$

Degree of cyclization (DC) was calculated and inclusion of 5-ME and 6-ME brGDGTs is discretely mentioned (modified after Sinninghe Damsté et al., 2009):

(14) $$DC = \frac{Ib + IIb + IIb'}{Ia + IIa + IIa' + Ib + IIb + IIb'}$$

The distribution of isoGDGTs was separately examined to evaluate possible effects of significant methanogenic bacteria and thermophilic archaea contributions.

Ring index (RI)

The Ring Index (RI) is defined as the weighted average of cyclopentane moieties in isoGDGTs and was calculated following Pearson et al. (2004) and Zhang et al. (2016). The relative weight of each compound is determined by the number of cyclopentane rings (note: hence, the abundance of GDGT-0 has no effect on RI):

$$\text{RI} = [\text{GDGT1}] + 2 \cdot [\text{GDGT2}] + 3 \cdot [\text{GDGT3}] + 4 \cdot [\text{Cren}] \quad (15)$$

GDGT-0/Cren

The ratio of GDGT-0 versus Crenarchaeol has been proposed to be indicative of significant input by methanogenic archaea. The ratio was calculated following Blaga et al. (2009):

$$\frac{\text{GDGT0}}{\text{Cren}} \quad (16)$$

3.5 Data processing and statistical analysis

Data processing and statistical analysis was done using software package R. A principle component (PCA)-analysis was carried out on the fractional abundances of branched GDGTs (i.e. the abundance of each brGDGT normalized to the total sum of brGDGTs), as described by De Jonge et al. (2015a, 2015b, 2016). Samples containing less than 7 of the total of 15 brGDGTs were excluded from analysis, additionally, brGDGTs IIIc was removed as it was absent in most of the samples.

ArcGIS 10.3.1 software was used for generating spatial distribution maps and consequential spatial analysis.

4 Results and interpretation

4.1Environmental parameters and geochemical river water analysis

4.1.1 Hydrogen (δD) and oxygen isotopes ($\delta^{18}O$)

Analysis of δD and $\delta^{18}O$ from river water (Figure 10) showed that substantially lower values were exhibited during the monsoon season. The dry season (n = 52) δD and $\delta^{18}O$ averages (± standard deviation) were –6.3 ± 10.6 and –0.2 ± 2.0 ‰, while during monsoon season (n = 57) these were -16.0 ± 15.8 and -2.2 ± 2.5 ‰, respectively. While these values already indicated a significant difference between both seasons, stronger differences were exhibited on the (north-) eastern side of the Godavari catchment area. δD and $\delta^{18}O$ values in the (north-)eastern region reached as low as -56 and -15‰ during the monsoon season, while during the dry season values only reached as low as – 23 ‰ and -6 ‰, respectively. In the western area, there seemed to be limited variation in both δD and $\delta^{18}O$ between both seasons. There was an explicit east-west increasing trend in both δD and $\delta^{18}O$, this also accounted for most of the relatively high standard deviations in the measured δD and $\delta^{18}O$ values.

The spatial and temporal distribution of oxygen and hydrogen sTable isotopes have been widely applied to differentiate between moisture sources in regional hydrology (Jeelani et al, 2013; references therein) or study its local circulation (for a review on the mechanism of fractionation and the application of sTable water isotopes see Gat, 1996). The isotopic signature of river water should aid in determining these variations for the Godavari catchment and show how these are affected by the monsoon system.

Especially the north-eastern area of the catchment displayed a distinctively different distribution between both seasons. The substantially depleted (in heavier ^{18}O and ^{2}H) values in the monsoon season suggest a temporally different moisture source than during the dry season. In addition, the displayed gradient in the Godavari catchment (increasingly enriched (in heavier ^{18}O and ^{2}H)

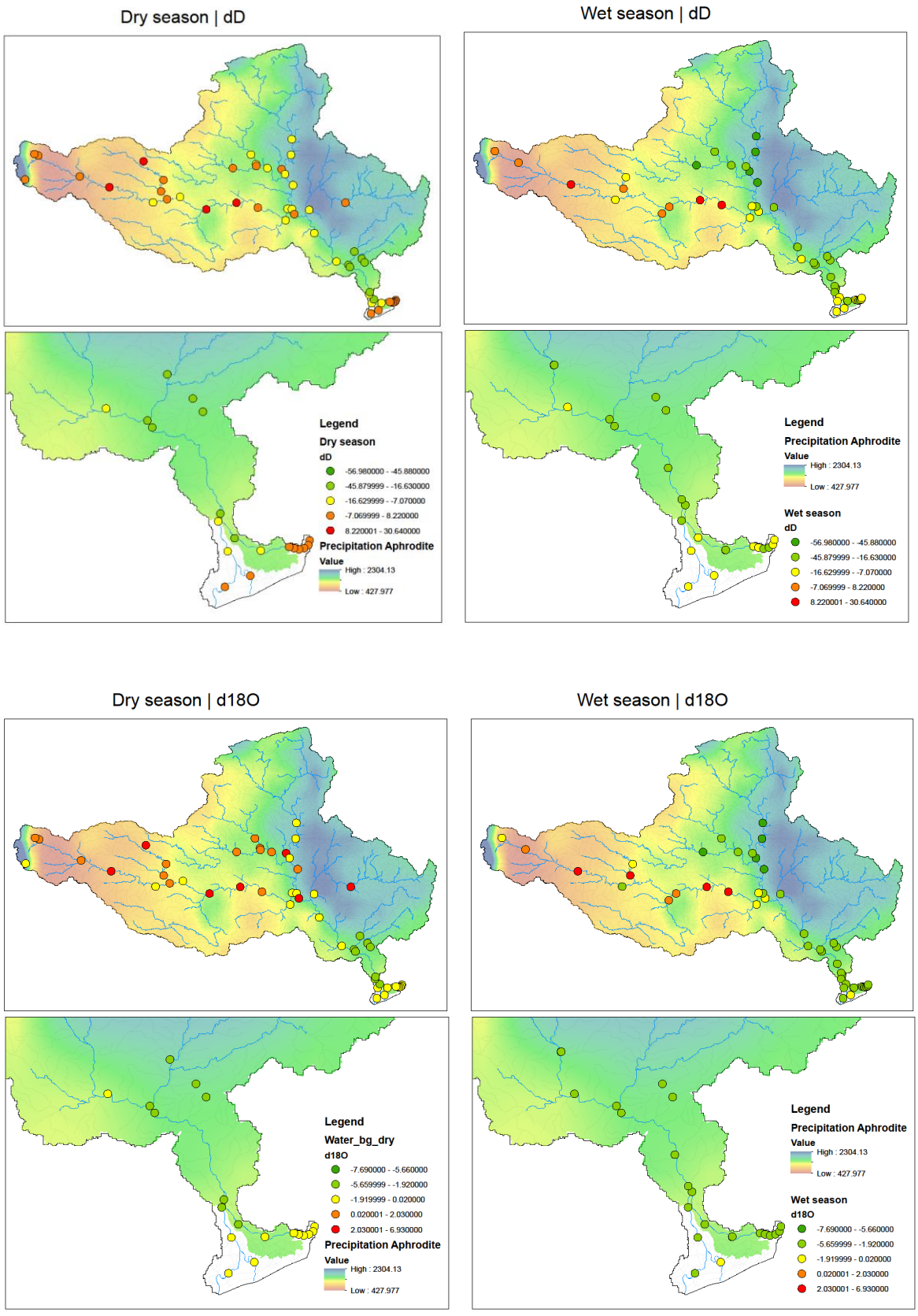

Figure 10 Hydrogen (upper) and oxygen isotopes (lower) in delta notation from river water for dry (left) and monsoon season (right). Background shows precipitation model data from APHRODITE (see section 2).

values from east to west) suggest that also during dry season, moisture to both regions is provided by different sources. Tripti et al. (2015) attribute this difference to dissimilar modes of ground-water recharging. Only the eastern area is under the influence of the north-eastern winter monsoon, whereas the upstream western area is characterized by strong evapotranspiration.

4.1.2 Sediment loading

The sediment loading of the Godavari River ranged from 0.002 – 1.436 gram SPM per litre water. The dry season was characterized by river water lacking any loading (only scarcely some SPM was measured) throughout the catchment area (***Figure 11***). The monsoon season sediment loading, however, was not only much higher in general (up to a factor 100 for some sites), but was also characterized by a compelling difference between the eastern and western area of the catchment. The western area was substantially lower in sediment yield, than the eastern and delta area.

The sediment loading in the Godavari River should shed some light on the degree of erosion and transport of sediment during both seasons. The high disparity in sediment load between them is characteristic for the monsoon driven Godavari River: on average (based on 1969-1980 daily observations), the monsoon season discharge is responsible for 98% of the reported average sediment transport of 170 x 10^9 kg sediment (Biksham & Subramanian, 1988).

4.1.3 Water temperature, pH and soil pH

The average water temperature at the sample sites in the Godavari catchment was 27.3 ± 4.8 °C and 29.6 ± 2.9 °C during the dry (n = 48) and monsoon (n = 52) season, respectively.
The average water pH at these sites was 8.39 ± 0.43 and 8.23 ± 0.30 for the dry and monsoon season, respectively. The most important observations were the slightly higher average pH in the dry season, regionally observed substantially (up to 0.6 units) higher pH during the dry season, and the relatively low pH in the delta region. The river water pH in the north-eastern part of the

catchment showed substantially more acidic values during the monsoon season, approximately 1 unit lower than during the dry season.

The Godavari soils (***Figure 14***) were characterized by a pH ranging from 5.98-9.32. Furthermore, a sharp segregation seemed to be present between upstream (generally alkaline soils, showed a pH between 7.3 and 9.3) and downstream soils (generally more acidic, showed a pH between 5.8 and 8.0).

To assess the properties and provenance of the SOC that is finally discharged into the Bay of Bengal, determining the environmental characteristics of Godavari soils and its spatial distribution throughout the catchment is an important step. Especially since the distribution of brGDGTs depends on soil pH (see section 1), this is one of the most important parameters to investigate. The sharp divide in soil pH between the more alkaline upstream and more acidic downstream part of the catchment seems to be a consequence of the underlying geology (see section 2). For the brGDGT distribution, this should result in a higher proportion of brGDGTs with one or more pentane moieties (i.e. those with a higher degree of cyclization) in the downstream part of the catchment.

Although the water temperature is somewhat higher during the monsoon season, this should be regarded with care as water temperature fluctuates daily.

The pH of river water is equally important to investigate, as it is possible that the brGDGT distribution associated with aquatic production reflects river water pH, rather than soil pH. The average river water pH presented here is in line with those reported by Subramanian (1979), although slightly more alkaline. The higher pH that is observed during dry season may be an artefact of increased CO_2 uptake by photosynthetic organisms. Aquatic primary production is most likely promoted during the dry season by low water velocity, reduced turbulence and consequently, a deeper photic zone. The relatively acidic values of river water in the north-

eastern area during the monsoon season may be the result from bacterial reworking of transported SOC. Sarma et al. (2011) report a substantial pH decrease (1.5 unit) in the Godavari river water during the monsoon peak discharge, accompanied by a 10-fold increase of CO_2 outgassing compared to the dry season situation. This suggests that SOC reworking during transport may be substantial in the Godavari River during the monsoon season, driving water pH to low values.

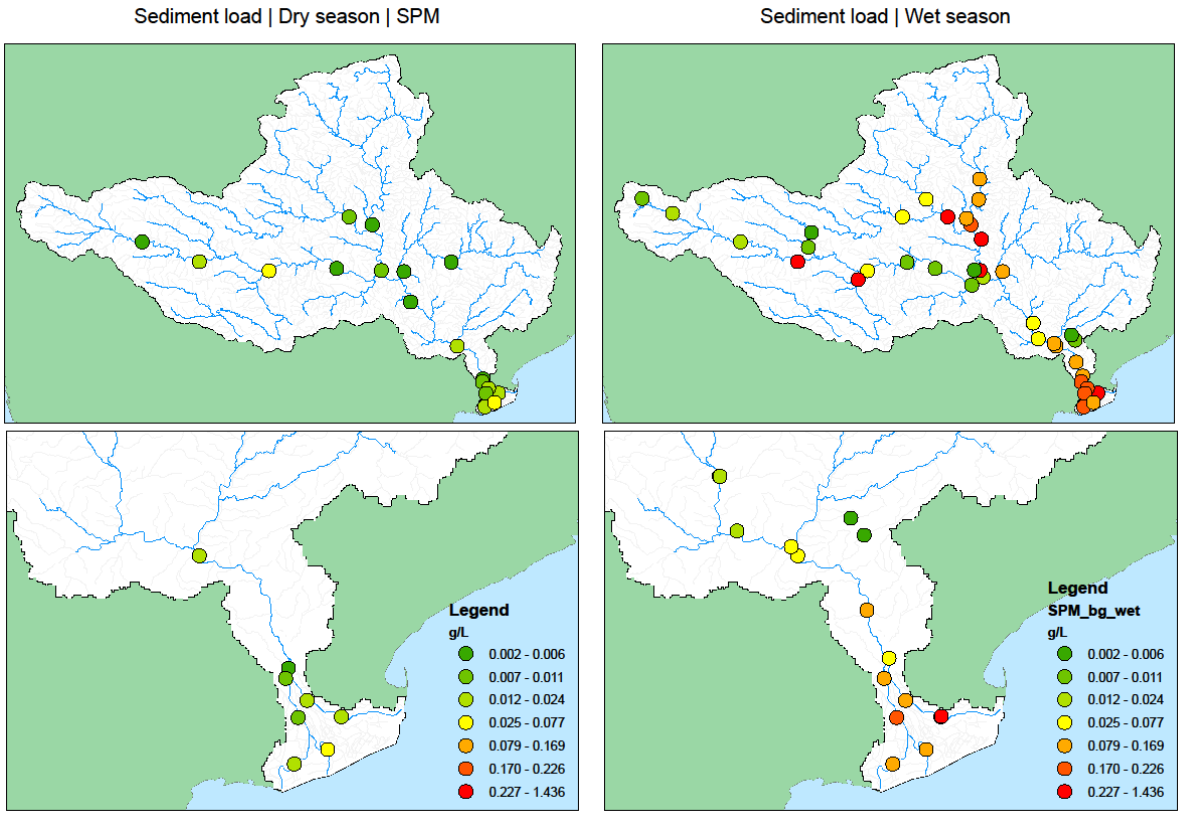

Figure 11 Sediment yield in gram/litre for the Godavari River in the monsoon (left) and dry season (right), respectively

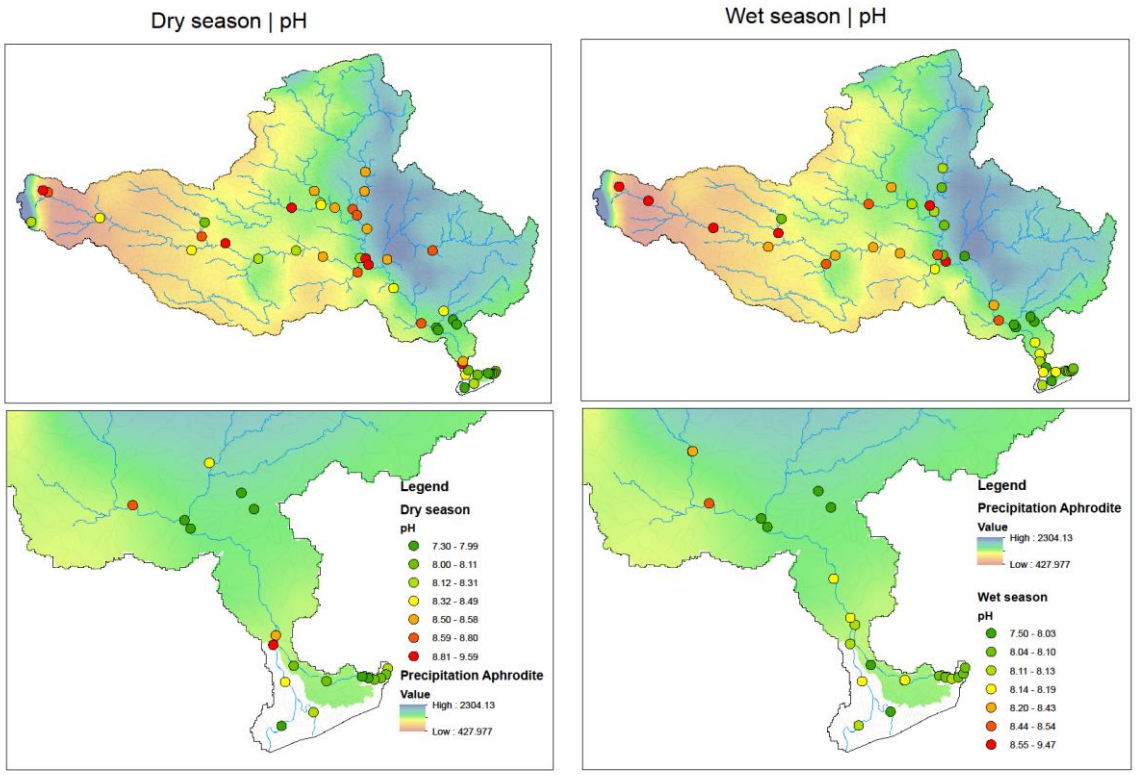

Figure 12 River water pH measured during the dry (left) and monsoon seasons (right)

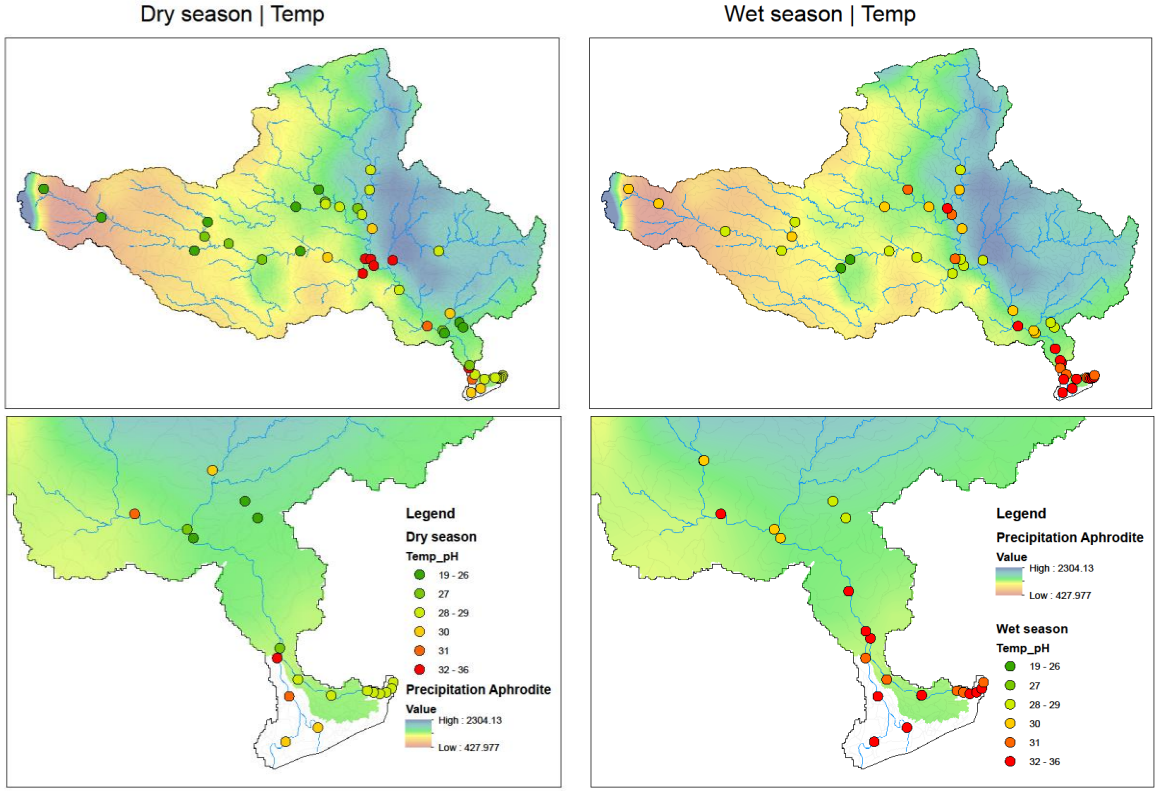

Figure 13 River water temperatures as measured in the dry (right) and monsoon season (left)

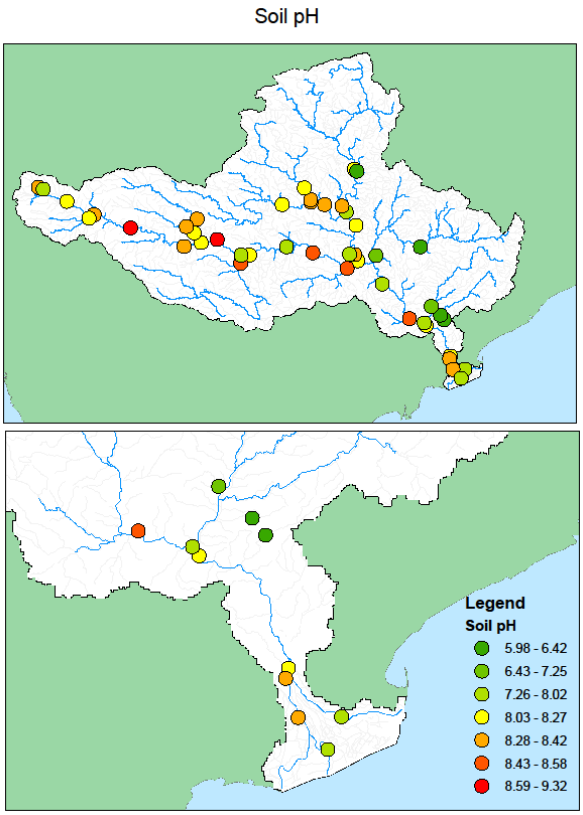

Figure 14 Soil pH in the Godavari catchment

4.1.4 Soil and river sediment organic carbon

The average total organic carbon (TOC) content of the collected soils (soil organic carbon, **SOC**) was 0.46 ± 0.27 wt%. Strikingly, the highest SOC found was only 1.17wt% and many of the soils were low in SOC. The spatial distribution of SOC showed no apparent pattern.

The average **TOC** content in the bulk river sediments (TOC_{sed}) was 0.44 ± 0.51 wt% and 0.28 ± 0.36 wt% for the monsoon and dry season, respectively. Especially the northern sediments seemed to be low in TOC compared to the delta region and western region sediments.

The spatial SOC distribution pattern within the catchment area appeared to be unrelated to the general soil type, underlying lithology or precipitation regime (see section 2.2). The average TOC_{sed} is very comparable to average SOC, especially during the wet season. However, their spatial distribution shows that this is not a catchment-wide phenomenon. In most of the western area the TOC_{sed} is very similar to the regional SOC, but the (north-) eastern area of the

catchment seems to strongly deviate from this pattern. In this region, the TOC_{sed} is considerably lower than the SOC. There is no substantial difference in absolute SOC between the eastern and western regions, therefore the cause for the observed difference in SOC-TOC_{sed} relation between both regions must be found elsewhere.

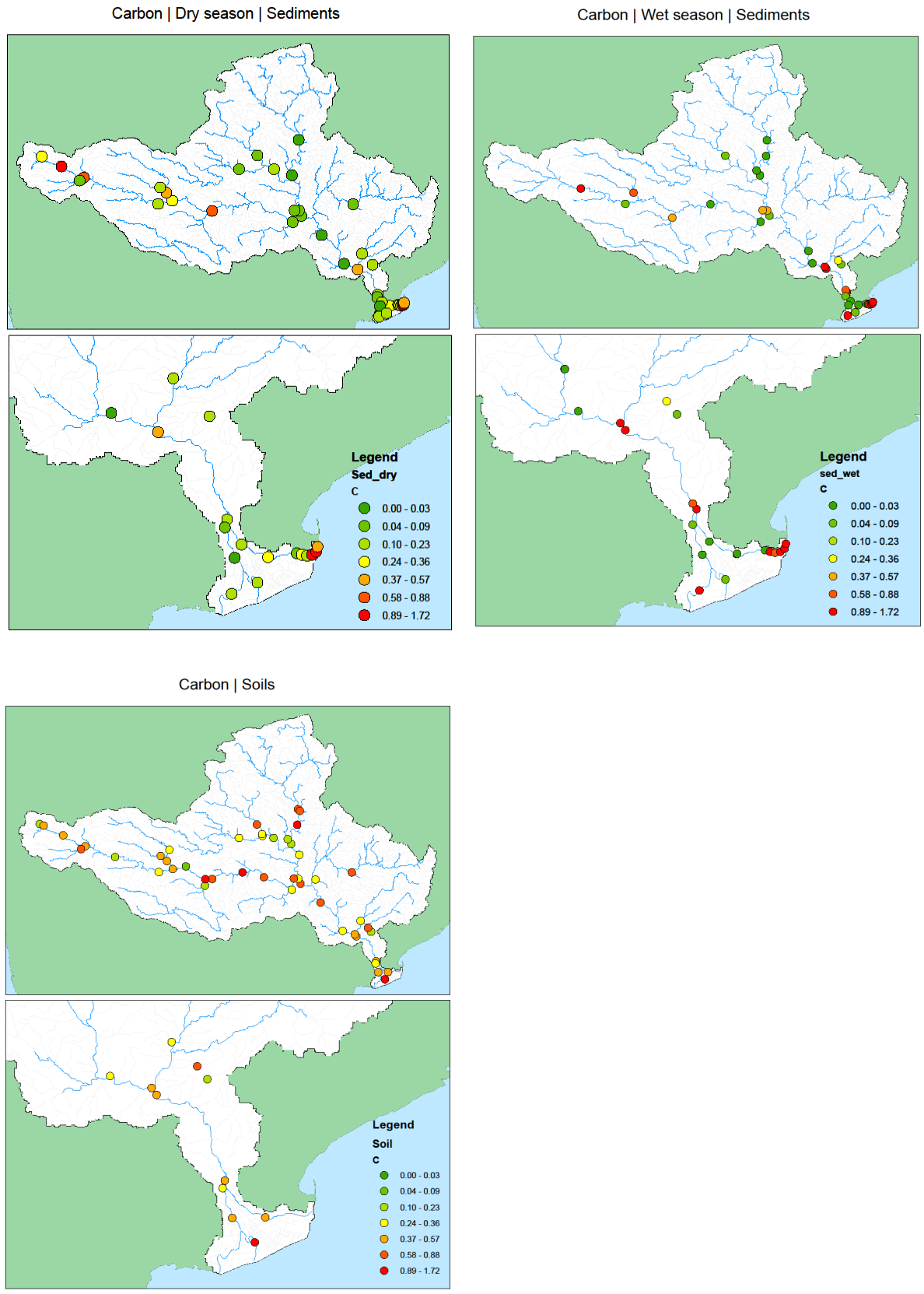

Figure 15 Total Organic Carbon distribution of river sediments (TOC_{sed}, upper) and soils (SOC, lower)

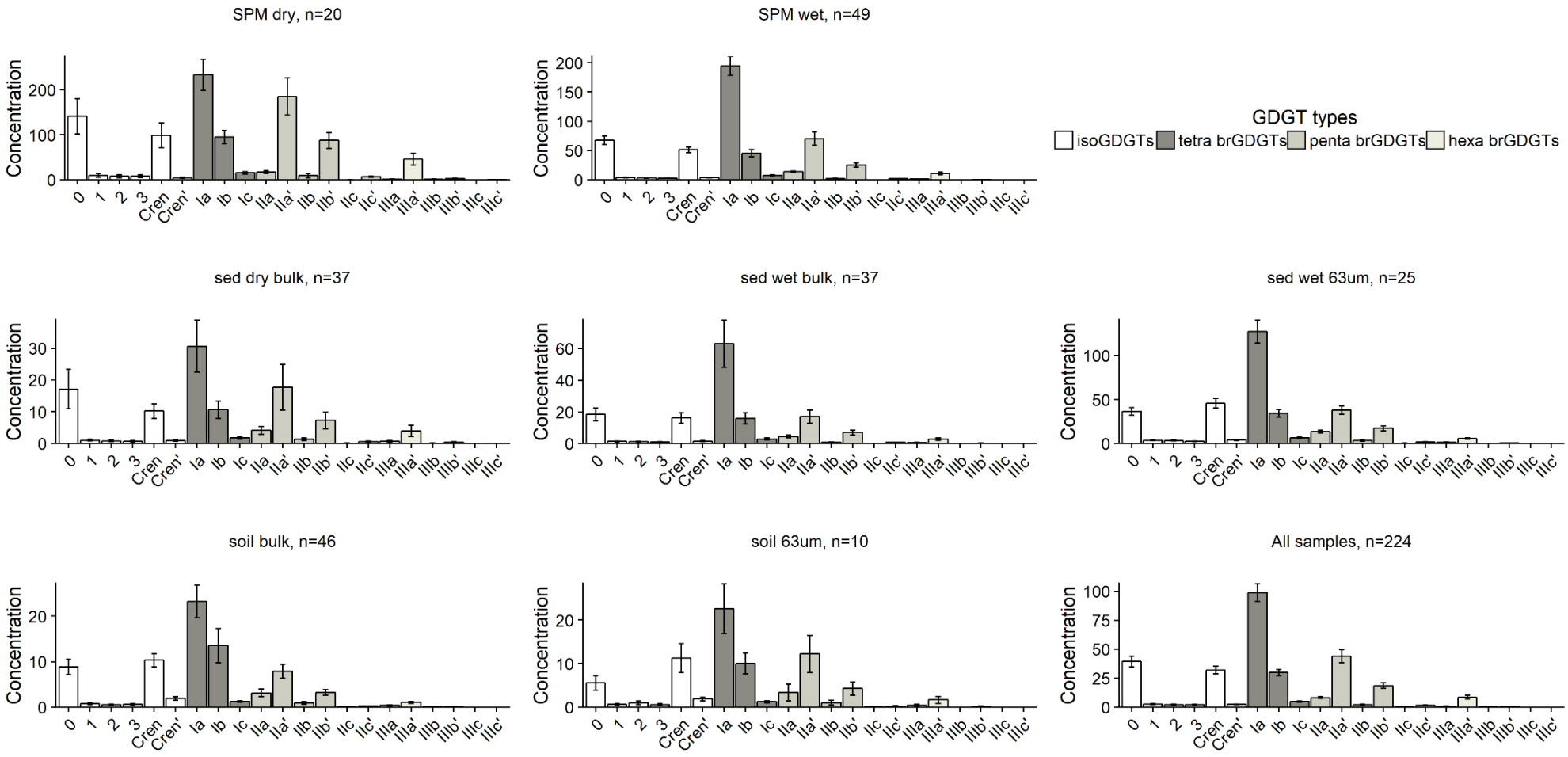

Figure 16 Average abundance in nanogram GDGT per gram sample (with each bar showing standard error) of brGDGTs and isoGDGTs, for each sample type. Note that the scale on the concentration axis is not equal for each sample type.

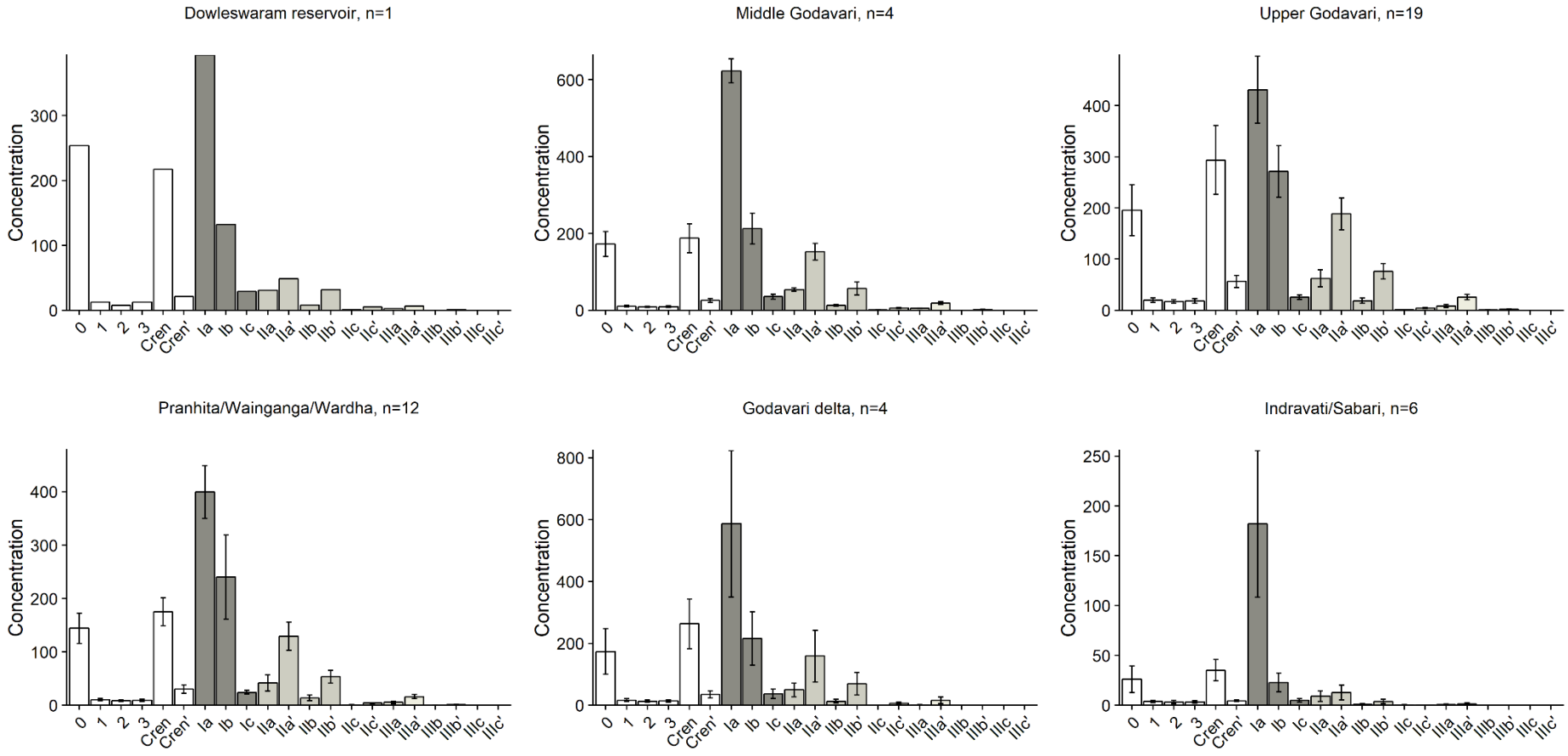

Figure 17 Regional variation in soil GDGT concentration. Note: concentration reported in nanogram GDGT per gram organic carbon for reference

4.2 Abundance of brGDGTs and isoGDGTs

For **all sample categories** combined, the average sum of all GDGTs and brGDGTs is 0.3 μg GDGTs/g sample and the standard deviation is 0.4 μg. Due to this high variability, the average concentrations for individual GDGTs are summarized in sample categories (***Figure 16***). Although GDGT concentrations are usually reported in ng GDGT per *gram carbon,* all concentrations here are reported in nanogram GDGT per *gram sample*. Otherwise, since TOC data is not available at this point for SPM samples, comparison between different sample types would become troublesome. For integrality, the calculated abundances in ng GDGT per gram carbon are available in the Supplement section, for all soil and sediment samples. In addition, the average brGDGT concentrations are plotted per sub-region in ***Figure 17*** (in ng GDGT per gram carbon) for direct comparison to other studies.

The concentration of individual GDGTs in **bulk soils** (n = 46) ranged from 0-20 ng GDGT/g sample. The most abundant GDGTs in soil samples, in sequence from highest to lowest average abundance, were brGDGTs Ia, Ib, IIa', isoGDGTs GDGT-0 and crenarchaeol (cren), and brGDGT IIa'. For the **63 μm fraction of the soils** (n = 10), these are also the most abundant GDGTs, in similar concentrations.

That the bulk soils and their 63 μm fractions do not exhibit a significant difference in average GDGT concentration is surprising. BrGDGTs supposedly form organo-mineral complexes with high surface area fine grained minerals (Peterse and Eglinton, 2017; and references therein) and thus a fine-grained fraction of the same soil, was expected to exhibit a higher GDGT concentration. Possibly, this is an artefact of the lack of normalization of GDGT concentration to OC content.

SPM samples (*n* = 69) showed average GDGT concentrations from 0-200 ng GDGT/g sample, an order of magnitude higher than in soil samples. The most abundant GDGTs in SPM samples were brGDGT Ia, IIa' and isoGDGTs GDGT-0 and cren during the monsoon season (*n* = 49). In the dry season (*n* = 20), these were also most abundant, although with a more dominant role of brGDGT IIa', along with brGDGTs Ib and IIb'. Whereas the distribution of GDGTs differed between the monsoon and dry season (for example, the relative contribution of brGDGT Ia was markedly higher during the monsoon season), the range of absolute concentrations were similar in both seasons.

Differences in absolute GDGT concentrations between SPM and soil samples are difficult to interpret. Whereas soils consist of a large mineral fraction, especially dry season SPM is almost void of sediment. Rather, it makes more sense to compare the distribution of different GDGTs. This is discussed more thoroughly in the next section. Already clear from the absolute concentrations, though, is that the distribution pattern of SPM samples in the monsoon season is more comparable to the soil distribution pattern, than the SPM samples from the dry season. That the monsoon season SPM carries a signal closely related to the soil signal, more than the dry season SPM, implies that soil brGDGTs are probably the main source for SPM during the monsoon season, whereas this may not be the case for the dry season SPM.

Bulk river sediment samples (*n* = 74) showed average GDGT concentrations ranging from 0-60 ng GDGT/g sample during the monsoon season (*n* = 37) and 0-30 ng GDGT/g sample during the dry season (*n* = 37). The most abundant GDGTs are very similar to those in SPM samples, also the different distribution between dry and monsoon season observed for SPM, is exhibited in the sediments, i.e. the more prominent role of brGDGTs IIa' at the cost of brGDGT Ia. The **63 µm fraction of the river sediments** (*n* = 25) showed substantially higher average absolute concentrations than the bulk sediments, up to a factor 2 higher. The most

abundant GDGTs were similar to those in bulk sediment: brGDGT Ia, IIa', isoGDGT GDGT-0 and cren were most abundant.

4.3 GDGT based proxies

In the following paragraphs, the result of three GDGT-based proxies (BIT index, MAT_{mr}, and reconstructed pH, as described in section 2) is presented and discussed. The description of these proxy results in this study is twofold: 1) they provide a summary of the most employed GDGT ratios and should give a first idea about the relative importance of each GDGT in different sample types and/or sub-regions, and 2) a comparison between the values of these proxies and measured environmental conditions can provide insight in the (dis-) functioning of these proxies under certain environmental conditions.

a) BIT index

The mean BIT index value (see equation [1] in section 3) per sample type (including standard deviation and range) is summarized in ***Table 1***. The geographical distribution of BIT different sample types is shown in ***Figure 18***. Between sample types, no substantial differences were displayed in mean BIT index value, although the values of SPM were somewhat higher than soil samples, especially during the monsoon season (0.84±0.06 versus 0.75±0.10, for SPM and soil samples, respectively).

The spatial distribution pattern of the BIT index of the Godavari soils, showed that the western soils exhibited lower values (generally <0.60) than the rest of the catchment (between 0.6 and 0.9) Whereas the SPM samples showed values similar to those of the soils in the eastern region, this was not the case in the western area; here the BIT index values were generally higher than for soil (i.e. relatively more brGDGTs than isoGDGTs). This was also valid for the sediments; the sediments in the eastern region showed more similarities to soil composition than the western sediments, especially during the monsoon season.

Firstly, as Schouten, et al. (2013) emphasize, the BIT index is a ratio and consequently variation in BIT index can be caused by variations of either brGDGTs or crenarchaeol only. The values exhibited by the soils were exceptionally low, however, considering that in climate reconstructions, the BIT value of terrestrial end-member organic matter was originally often assumed to be > 0.9 (Schouten et al., 2013). The relatively low BIT index found in the Godavari soils is most likely a result of the high abundance of crenarchaeol that was reported for these soils. For example, the average crenarchaeol concentration in the soils from the Upper Godavari region is the second highest GDGT in abundance, just after brGDGT Ia. Kim et al. (2010) equally found high abundances of crenarchaeol in soils from the Têt catchment area and they showed a strong correlation with more alkaline soils in these areas. The BIT-index value of soils seems to be driven by precipitation, as Dirghangi et al. (2013) studied a precipitation transect in the US and found that dry soils were predominantly characterized by thaumarchaeotal isoGDGTs (consequently, lower BIT index values, generally 0.2-0.6) and more temperate soils were predominantly distinguished by more brGDGTs (higher BIT-index values, generally 0.9-1). This relationship also seems viable for the Godavari catchment, as the drier Upper Godavari soils displayed the lowest BIT values in the catchment (and equally the highest crenarchaeol concentrations).

The effect of high crenarchaeol concentration lowering the BIT index seems to be weakened during transport, as BIT values for SPM are generally somewhat higher than for soils (see ***Table 1*** for details). Moreover, the low BIT index values exhibited of the Upper Godavari soils are not transferred to the SPM, these display much higher values (generally > 0.85) than the soils (0.4-0.8). This implies that either the river water GDGTs have their source elsewhere, at least in the western area, or the river water becomes enriched in brGDGTs during transport, relative to isoGDGTs.

Table 1 BIT index per sample type

Sample type and season	Mean	Standard deviation	Minimum	Maximum
Soil	0.75	0.1	0.52	0.91
SPM dry	0.77	0.18	0.47	0.96
SPM monsoon	0.84	0.06	0.62	0.96
Sediment dry	0.8	0.11	0.51	1
Sediment monsoon	0.78	0.12	0.44	0.93

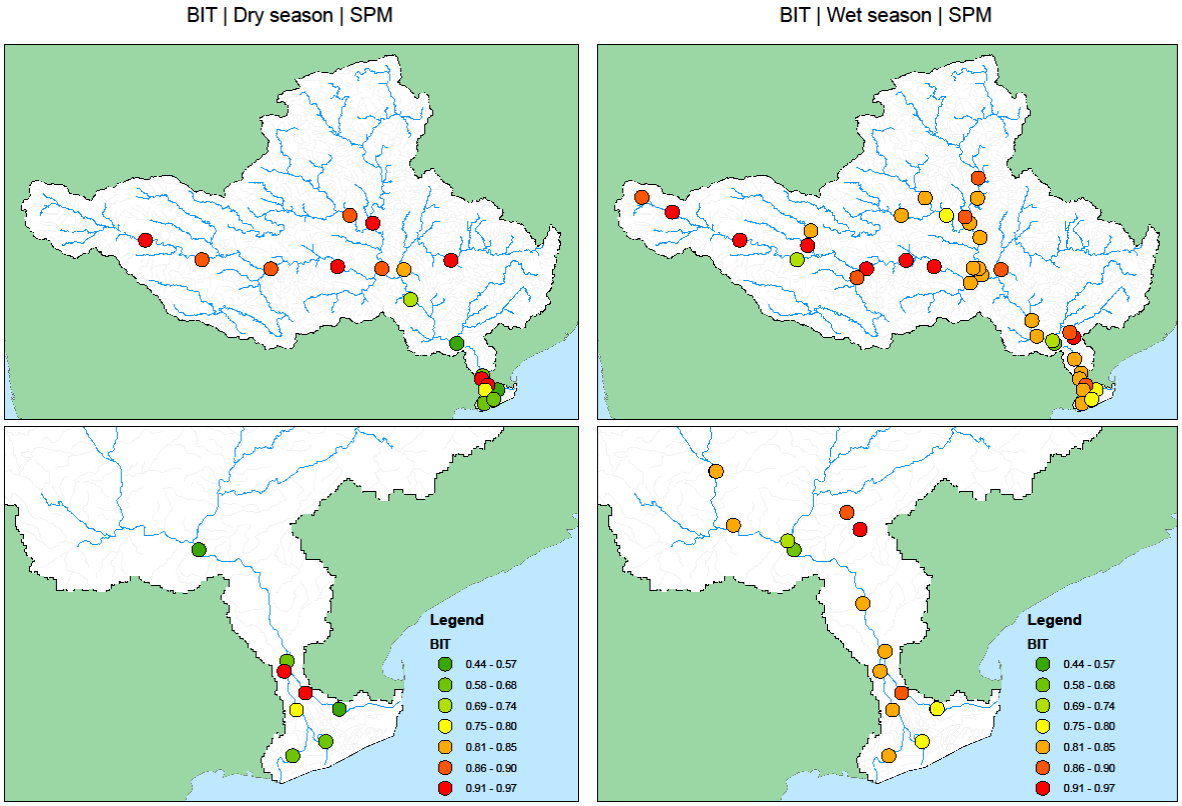

Figure 18 BIT index as calculated (equation [1] in section 2) throughout the catchment area. *Continues next page*.

BIT | Dry season | Sediments

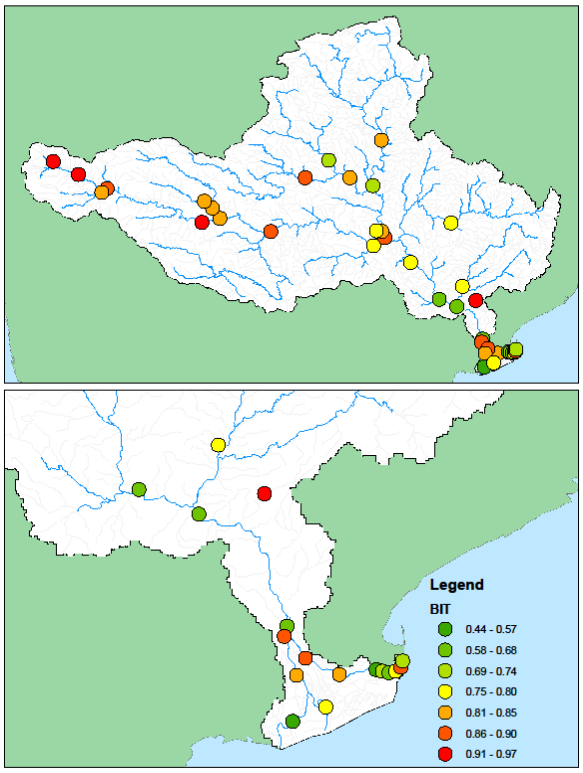

BIT | Wet season | Sediments

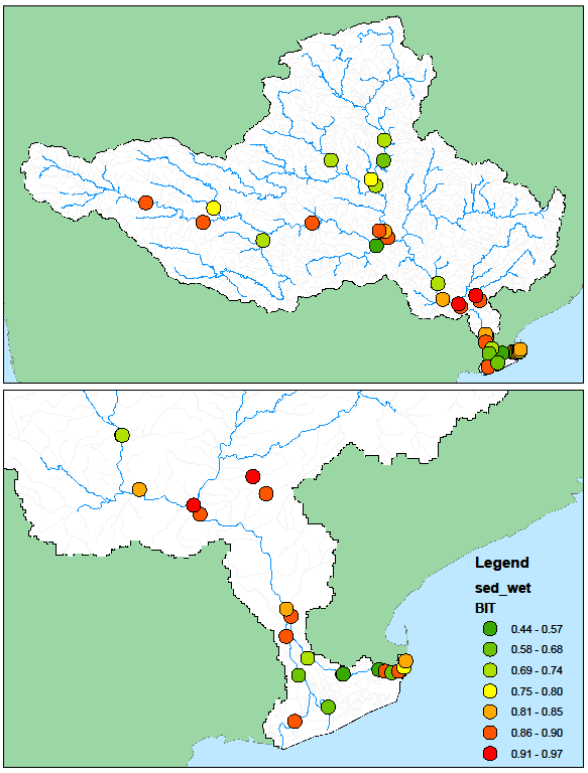

BIT | Soil

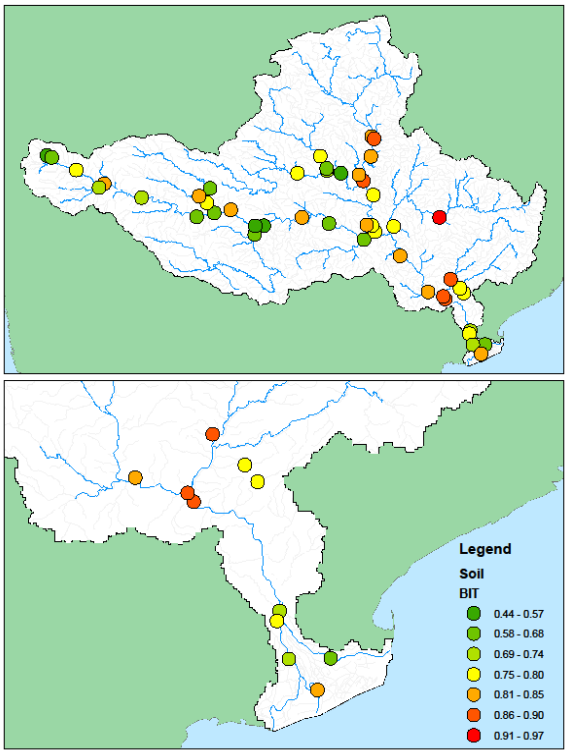

{**Figure 18** continued}

b) *Reconstructed mean annual temperature (MAT_{mr})*

The mean MAT_{mr} (equation [4] in section 3) is summarized per sample type in ***Table 2***. The spatial distribution of MAT_{mr} over the Godavari catchment is shown in ***Figure 19***. The reconstructed temperature based on soil brGDGT distribution suggested a temperature gradient over the Godavari catchment, increasing from east to west. This gradient was also to a lesser degree present in the Godavari SPM samples during the monsoon season, but not during the dry season.

Whereas the reconstructed temperatures for the north-eastern soils seemed to be within the error margin of the proxy (~5°C lower than actual MAAT), most of the reconstructed temperatures appeared to be considerably lower than actual MAAT. For example, the reconstructed temperatures from the soils from the Upper Godavari region showed values approximately 15 °C lower than the actual MAAT. Furthermore, the temperature gradient between the eastern and western side of the catchment as suggested by the proxy (up to Δ10 °C MAAT) is much more limited (if at all present, it does not exceed Δ2 °C MAAT).

An important consideration is the saturation of the proxy at 24-25 °C, as discussed by Naafs et al. (2017). Thus, the actual MAAT in the Godavari catchment (25-30 °C) is not likely to be reflected by the MAT_{mr} proxy. This proxy maximum is most likely the cause of the underestimation present in the reconstructed values. Regardless, the discrepancy between actual and reconstructed MAAT shown in the Upper Godavari region cannot be attributed to this 'proxy maximum', as the proxy does not seem to be saturated here (it shows 15-20 °C values). The low reconstructed temperatures here are more likely to be a result of the arid nature of the western Godavari soils, as water availability has shown to bias the performance of the MAT_{mr} proxy (Menges et al., 2013; De Jonge et al., 2014; Naafs et al., 2017). Dang et al. (2016) suggest that the methylation of 6-Me brGDGTs (MAT_{mr} does not include 6-Me brGDGTs but is solely based on 5-Me brGDGTs, see equation [4])

Table 2 Reconstructed MAT in ºC

Sample type and season	Mean	Standard deviation	Minimum	Maximum
Soil	20.93	1.92	15.21	24.46
SPM dry	17.44	2.01	13.99	20.9
SPM monsoon	19.29	1.61	15.97	22.49
Sediment dry	18.34	2.52	11.12	21.24
Sediment monsoon	19.94	1.6	14.98	24.05

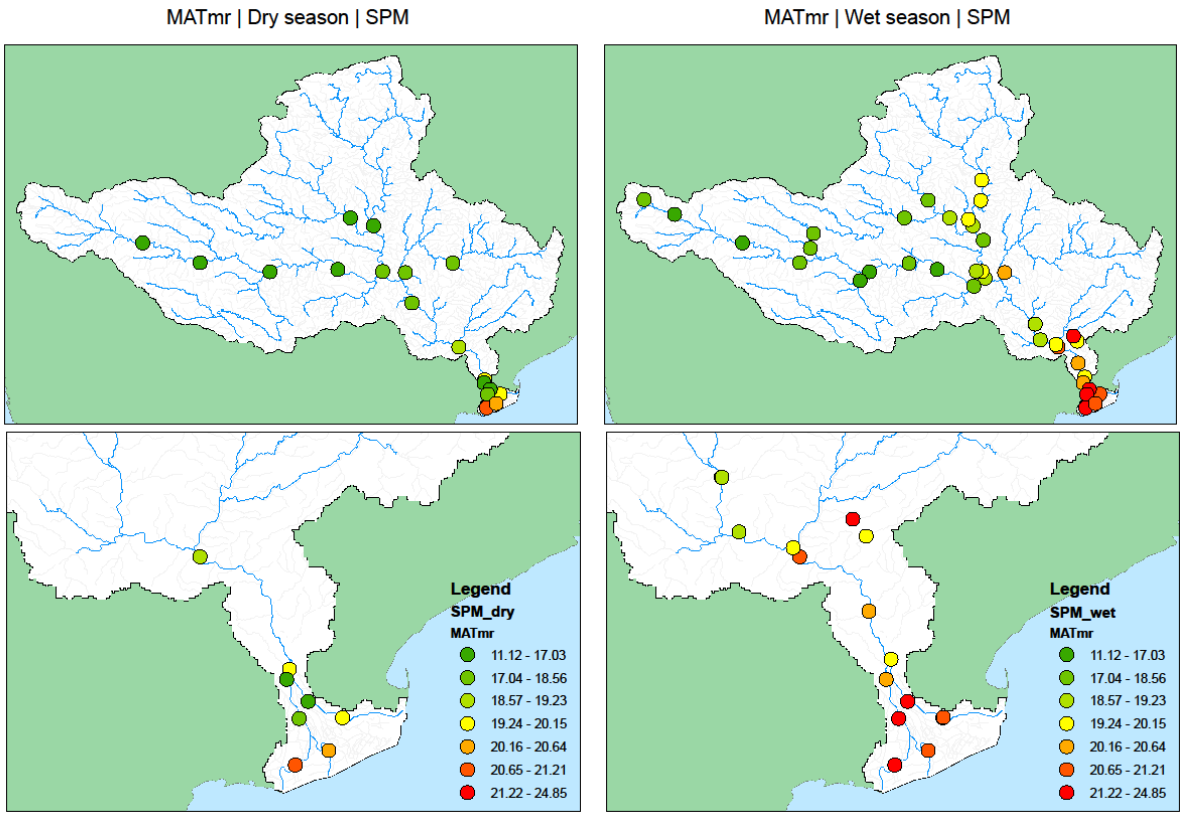

Figure 19 Reconstructed MAT *{continues next page}*

MATmr | Dry season | Sediments

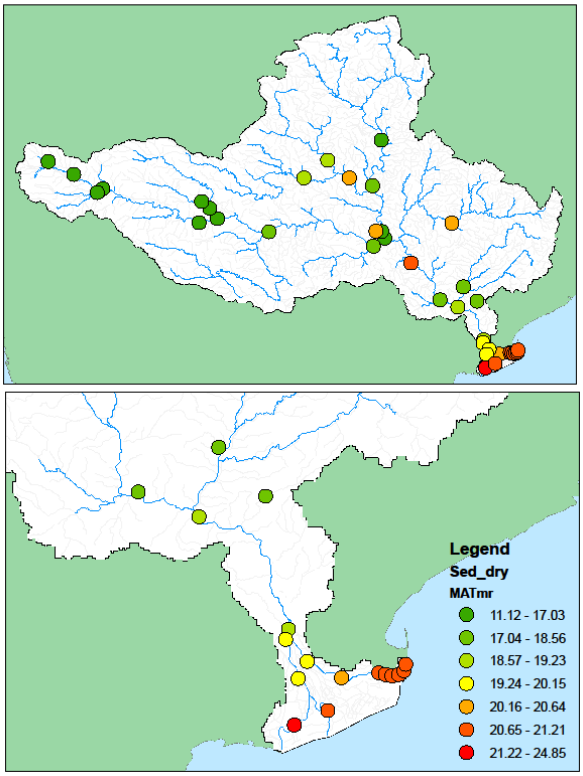

MATmr | Wet season | Sediments

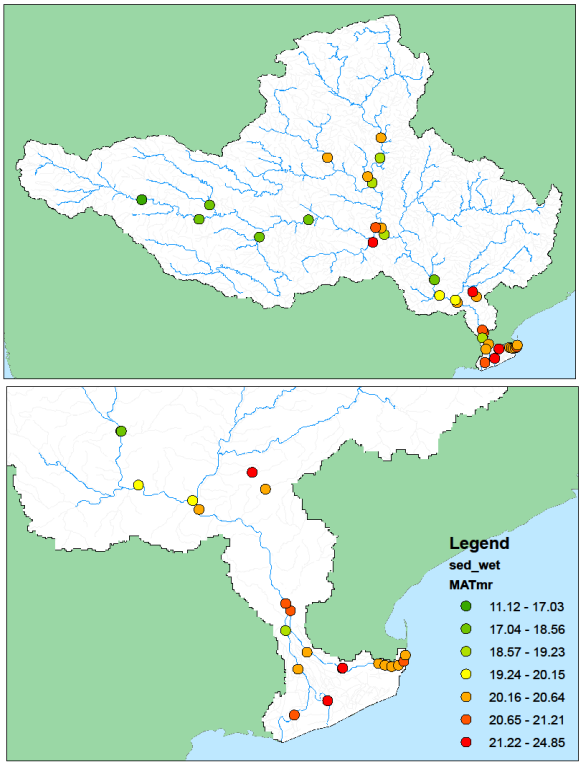

MATmr | Soils

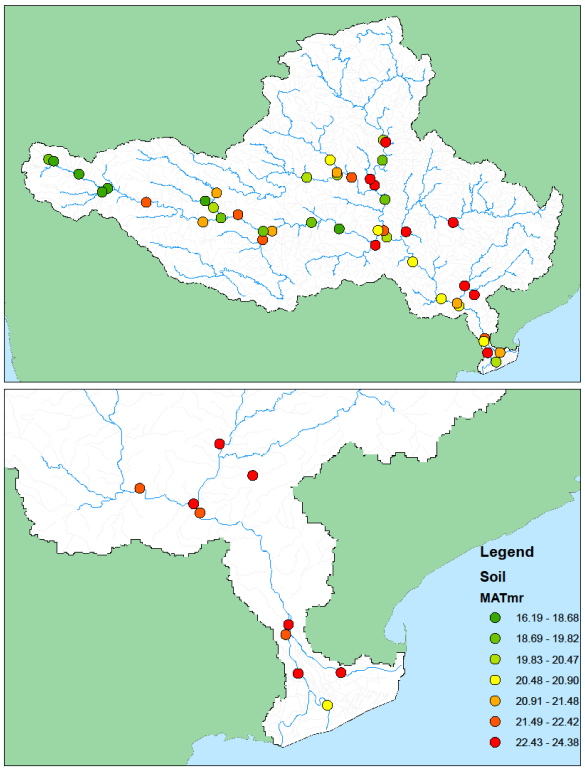

{**Figure 19** continued

c) Reconstructed pH

A summary of mean reconstructed pH values per sample type and season is presented in ***Table 3***. The distribution of reconstructed pH over the Godavari catchment is shown in ***Figure 20***. Reconstructed soil pH was relatively low, compared to the measured soil pH (mean 6.48±0.57 for the reconstructed pH, vs 8.01±0.66 for the measured soil pH). However, the geographical divide (western relatively alkaline soils, vs eastern relatively acidic soils) seemed to be captured by the proxy. Also, a distinct difference between the dry and monsoon season values for SPM samples was present. Whereas the entire catchment was characterized by relatively high reconstructed pH values (based on SPM brGDGT distribution) during the dry season, the monsoon season pH values were approximately 0.5-unit lower (mean 7.18±0.31 versus 6.60±0.42 for dry and monsoon season, respectively).

That the Godavari soil pH is substantially underestimated by the proxy is more evident from ***Figure 21***, all soils plot well below the 1:1-line (red circles in Figure 20). It becomes evident that CBT' based pH reconstruction is not very accurate in capturing soil pH variations for the alkaline Godavari soils, but also slightly underestimates the more acidic soils (for completeness, CBT' has been plotted versus measured pH in ***Figure 22***).

Table 3 Reconstructed pH per sample type

Type and season	mean	minimum	maximum	Standard deviation
Soil	6.48	4.51	7.12	0.57
SPM dry	7.18	6.53	7.73	0.31
SPM monsoon	6.6	5.78	7.35	0.42
Sediment dry	7.06	6.33	7.87	0.45
Sediment monsoon	6.81	5.82	7.73	0.46

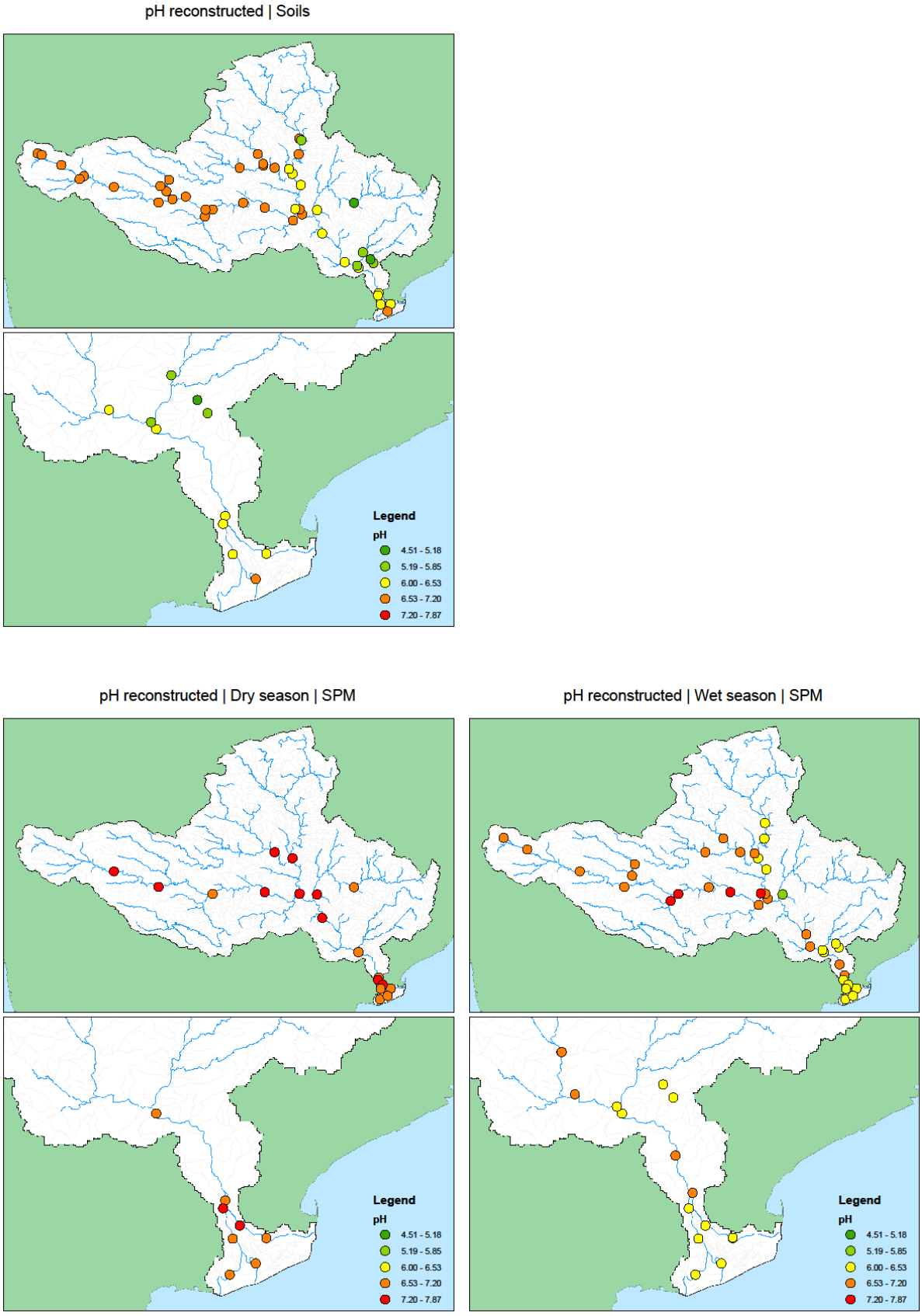

Figure 20 Reconstructed pH based on equation [2] and [3], continues next page

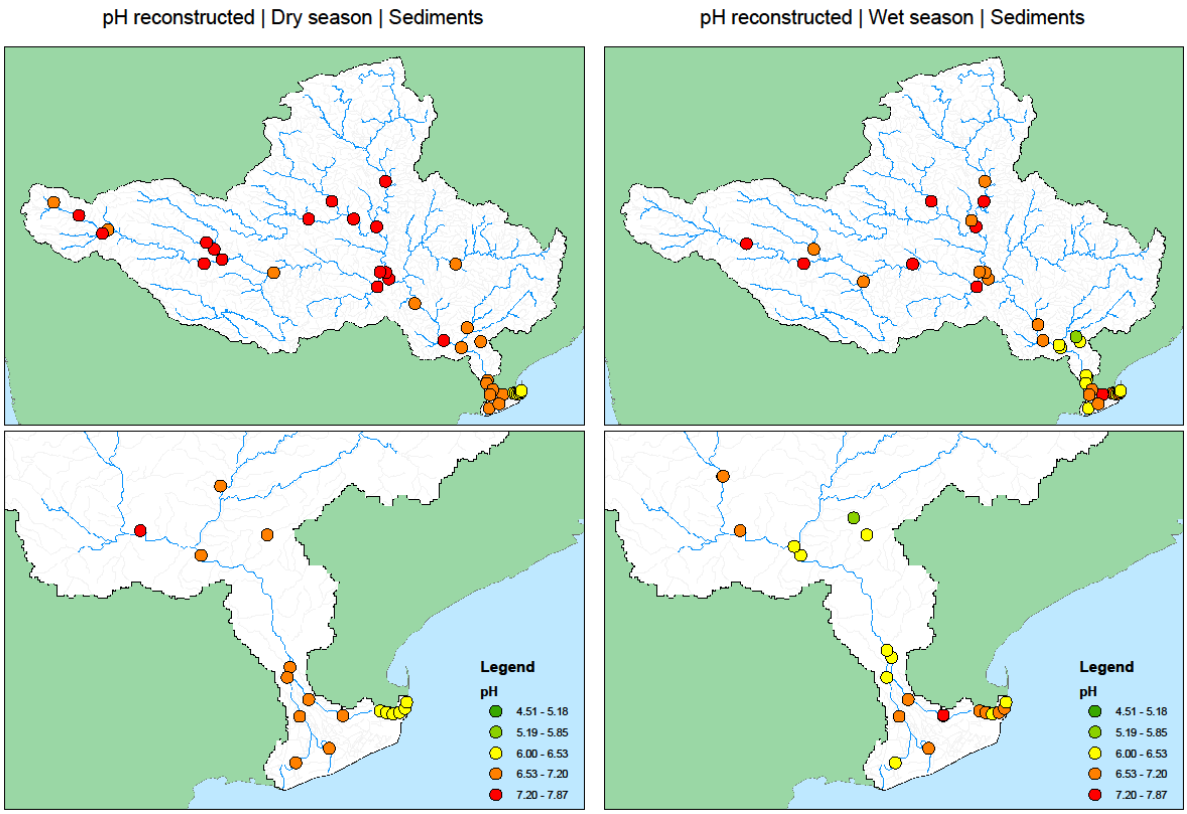

Figure 20 continued

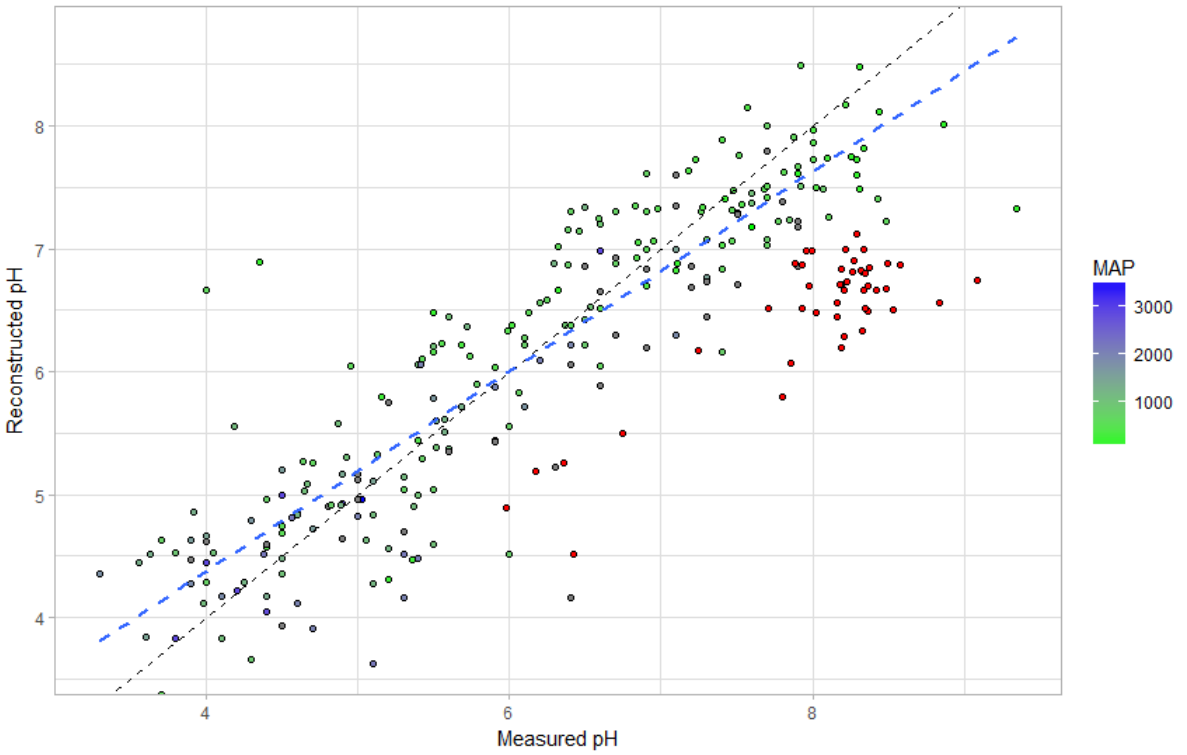

Figure 21 Reconstructed soil pH versus measured soil pH. Blue-green circles are data from the De Jonge et al. (2014) dataset (colour represents MAP), red circles are data from this study (no MAP data). Dashed black line represents 1:1 relationship, whereas dashed blue line represents a smoothed linear relationship for which the data from this study is included.

In addition to soil pH, in aquatic settings the reconstructed pH (based on brGDGT distribution of SPM and using equations [2] and [3]) has shown to be able to capture pH variation in the water column (Schouten et al., 2013; and references therein). A previous study in the Yenisei River has shown that pH reconstructed from brGDGTs originating from SPM can mimic river water pH (De Jonge et al., 2013) rather than soil pH. ***Figure 23*** shows reconstructed water pH levels, based on the brGDGT distribution in Godavari River SPM, and the measured pH values of river water at the SPM sampling location. This shows the offset between dry and monsoon season reconstructed pH and how the western Godavari samples plot in the same region in both seasons. Possibly, the offset is explained by aquatic production. Whereas during the dry season, water pH is recorded (although with an offset of ~1 unit) by aquatic production, during the monsoon season this is overprinted (in the eastern region) by the low-pH soil signal.

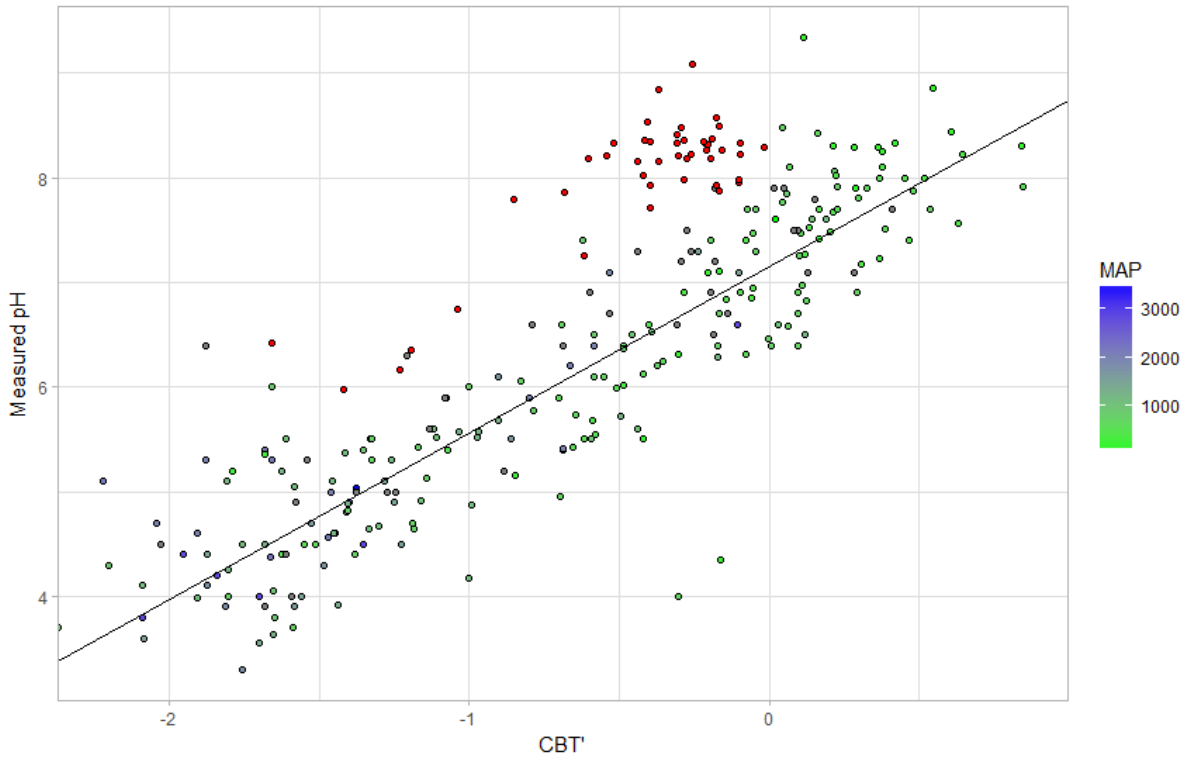

Figure 22 Relation between CBT' and measured pH. Red dots are soil samples from this study, the blue-green dots are samples from the De Jonge-dataset (2014). The black line represents the relation between CBT'and pH as suggested by the calibration by De Jonge et al. (2014).

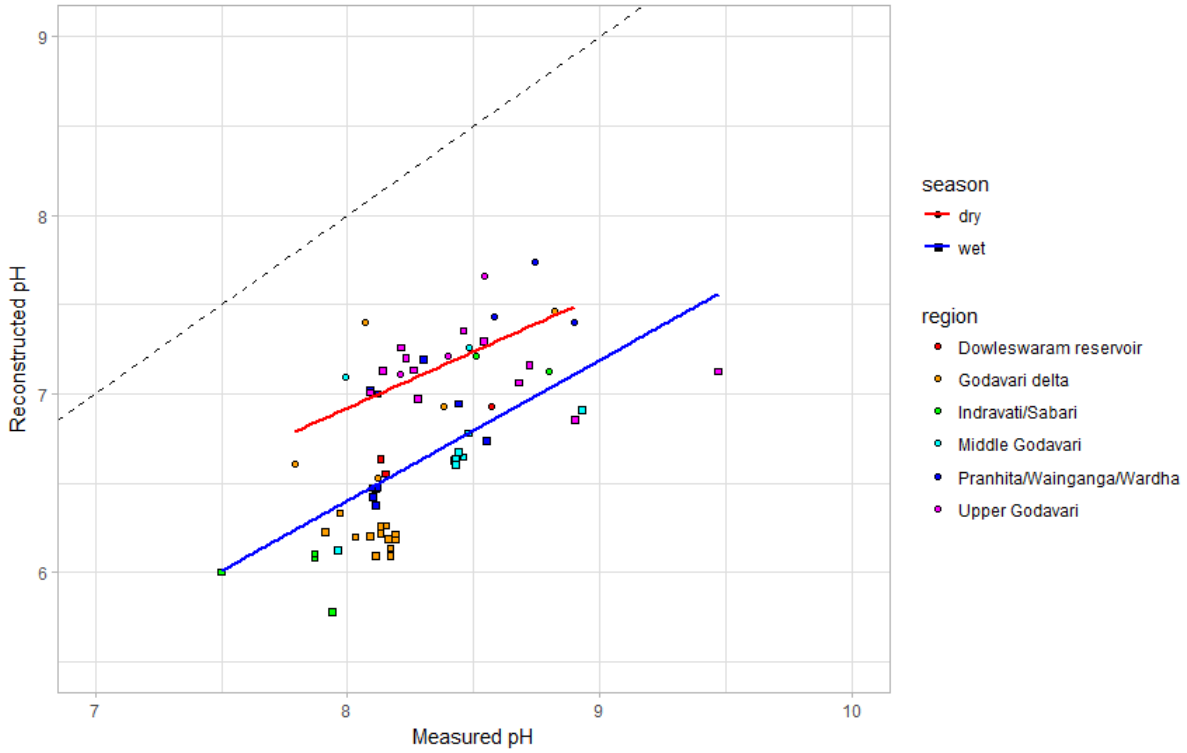

Figure 23 Reconstructed water pH levels (based on SPM brGDGT distribution) versus measured pH levels. Circles represent data from the monsoon season, squares are data from the dry season. Colour coding is based on region. The dashed line shows the 1:1-line, whereas the blue and red lines show smoothed linear relations between reconstructed and measured pH, for the monsoon and dry season, respectively.

4.4 Distribution of brGDGTs

Although the average relative contribution of each brGDGT can also be extracted from ***Figure 16***, their fractional abundance (***Figure 24***, i.e. the abundance of each brGDGT divided by the total sum of brGDGTs) makes it considerably easier to compare differences between sample types and eventually evaluate the brGDGT signal throughout the catchment area.

From ***Figure 24***, it could be observed that brGDGTs Ia, Ib and IIa' were the most abundant (and brGDGT IIb' to a lesser degree) brGDGTs. As already observed in the previous section, their distribution is not uniform

To further evaluate the contribution and variation in spatial distribution of each of these brGDGTs, they were plotted in a ternary diagram (***Figure 25***).

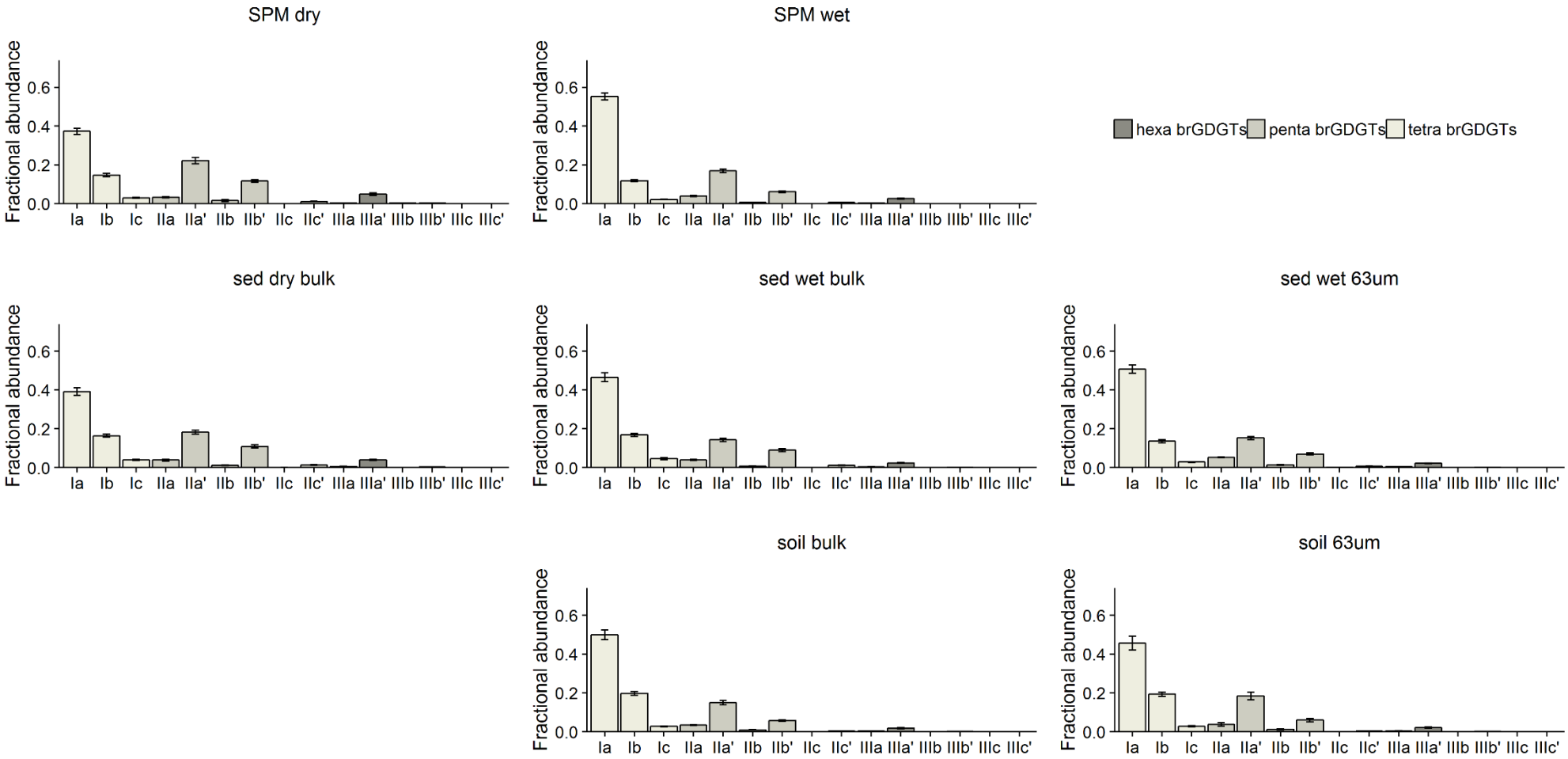

Figure 24 Distribution of brGDGTs for each sample type, reported as fractional abundance of the sum of brGDGTs (i.e. the sum of all fractions equals 1)

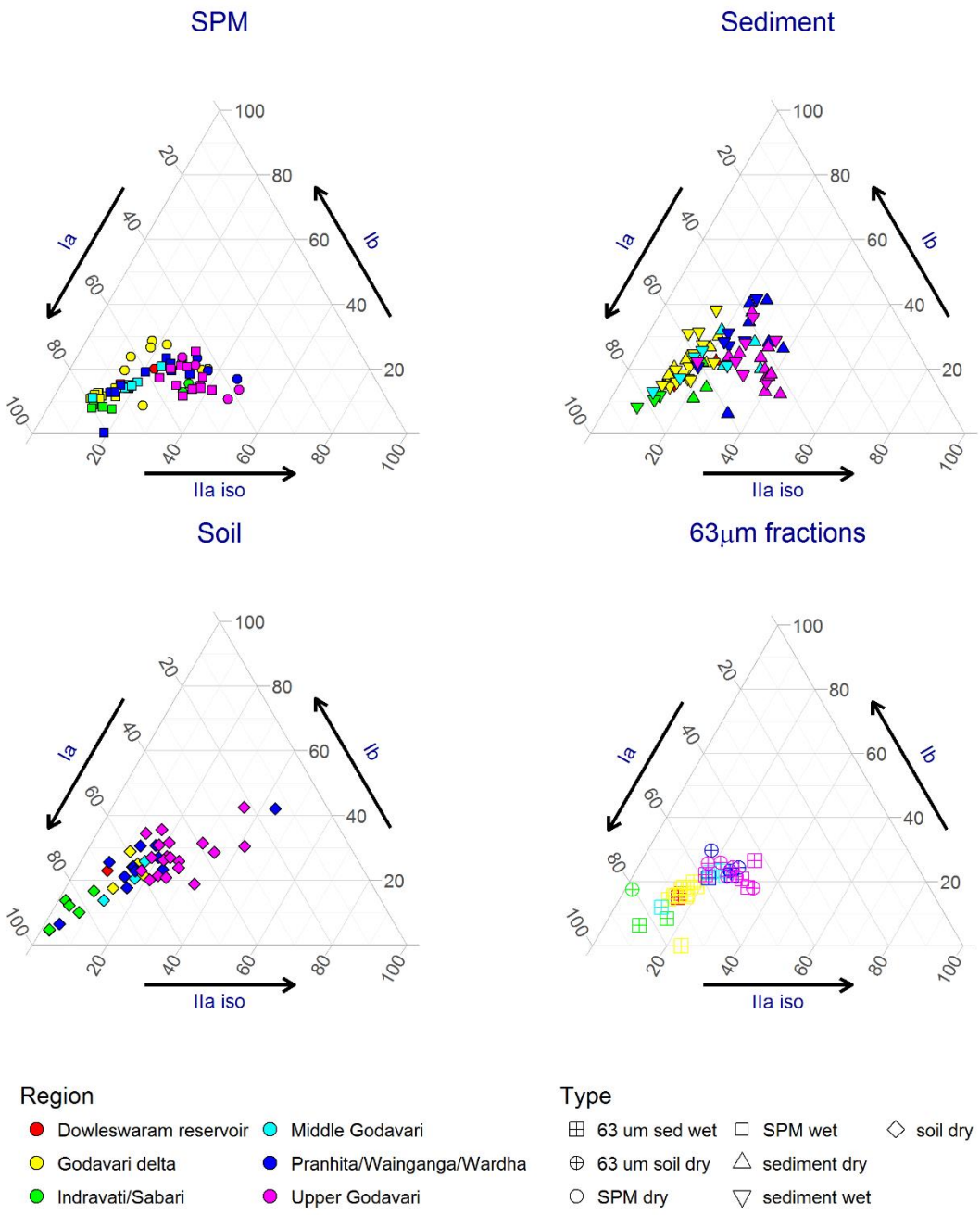

Figure 25 Ternary diagram of contribution of the three most abundant brGDGTs: Ia, Ib and IIa' Note how the distribution of these three brGDGTs is highly bound to region. Especially for soil samples this is evident. Note on ternary diagrams: the percentage shown is

Here, it became evident that the distribution of these brGDGTs in **soil samples** is highly bound to region. samples belonging to the same region showed clustering. The contribution of brGDGT IIa' and Ib in soil samples seemed to increase towards the western region, at the expense of brGDGT Ia. Whereas in the north-eastern part of the catchment (Indravati/Sabari) region especially, and the northern (Pranhita/Wainganga/Wardha) region to some degree) the

soil was comprised of almost completely brGDGT Ia, while in the western part of the catchment (Upper Godavari region) this was considerably less and the contribution of brGDGT IIa' increased exponentially.

SPM samples in general showed lower variation in the contribution of brGDGT Ib (this was also observable from ***Figure 24***) than the soil samples. Also, there seemed to be an offset present between SPM dry season and monsoon season samples.

4.5 Numerical statistical analysis

To explore further for significant changes in brGDGT distribution and general relationships between different sample types and their geographical distribution, I performed a Principal Component Analysis (PCA) on the fractional abundances of brGDGTs at each sampling site. Samples for which more than seven brGDGTs were not measured, were excluded from the PCA to avoid a bias (following De Jonge et al., 2015a).

When all samples were combined in a single PCA (***Figure 26*** and ***Figure 27***), the first three principle components (PC1, 2 and 3) explained 31.4%, 20.8% and 12.9% of the variance, respectively. The loadings of the variables were relatively low compared to the individual sample scores, further indicating high variation between different samples (or types). PC1 displayed a strong inverse relationship between positively scoring fraction of brGDGTs Ia (and IIa, IIIa and IIc a lesser degree) on one hand, and negatively scoring fractions of brGDGTs IIa', IIb', IIc', IIIa' and IIIc' (and Ib, Ic, IIb and IIIb to a lesser degree) on the other hand, seemingly able to capture degree of isomerisation. This inverse relationship between the fractions of brGDGT Ia and 6-Me brGDGTs IIa' and IIb' was confirmed by the high r^2 values (r^2 = 0.54 and 0.70 between Ia and IIa', and between Ia and IIb', respectively). The fractions of brGDGTs IIa' and IIIa' (r^2 = 0.70) and IIb' and IIc' (r^2 = 0.67) also seemed to be closely related.

PC2 exhibited an inverse relation between brGDGTs Ib, Ic on one hand (IIb' and IIc' to a lesser degree), scoring negatively, and IIIa, IIb, IIc and IIIb on the other hand (IIa, IIIa' and IIIb') to a lesser degree), scoring positively.

The respective loadings on PC3 were smaller than on PC2, most likely due to the small amount of variance explained by PC3. The fractions of brGDGT Ib, Ic and IIc' scored relatively high on PC3 and showed to be reasonably correlated (up to $r^2 = 0.52$ between Ic and IIc'). Scoring negatively on PC3, especially IIa' and IIIa' still showed high resemblance.

A trend appeared to be present in the geographical distribution: whereas samples from the Upper Godavari scored negatively on PC1, samples from the eastern (mainly Indravati and Sabari) region scored positively on PC1. This was associated with an increasing dominance of brGDGT Ia, mainly at the cost of the 6-Me brGDGTs. The relatively positive scores on PC1 of samples from the Godavari delta and their closer resemblance with samples from the eastern regions, suggested a higher contribution from the eastern region than from the further upstream western area.

To reduce variability due to sample type, in addition to the PCA for all samples combined, I also separately performed PCA analyses for sample sub-sets, one for each sample type and/or season. The results are plotted in ***Figure 28*** and **Figure 29** and will be discussed in the following paragraphs.

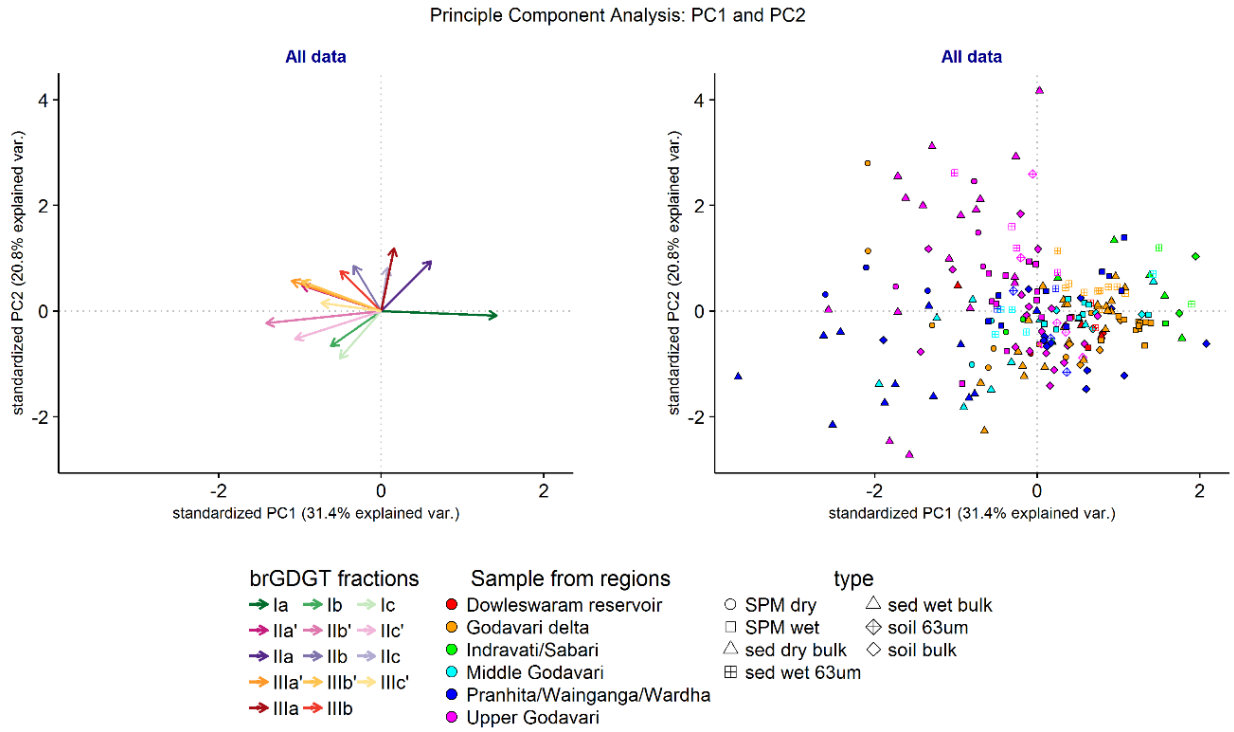

Figure 26 Results from the PCA analysis for all samples combined, plotted on the first and secondary principle component axes (PC1 and PC2, respectively). Note how low the scorings on both axes are for the different brGDGT fractions, compared to where the different samples plot.

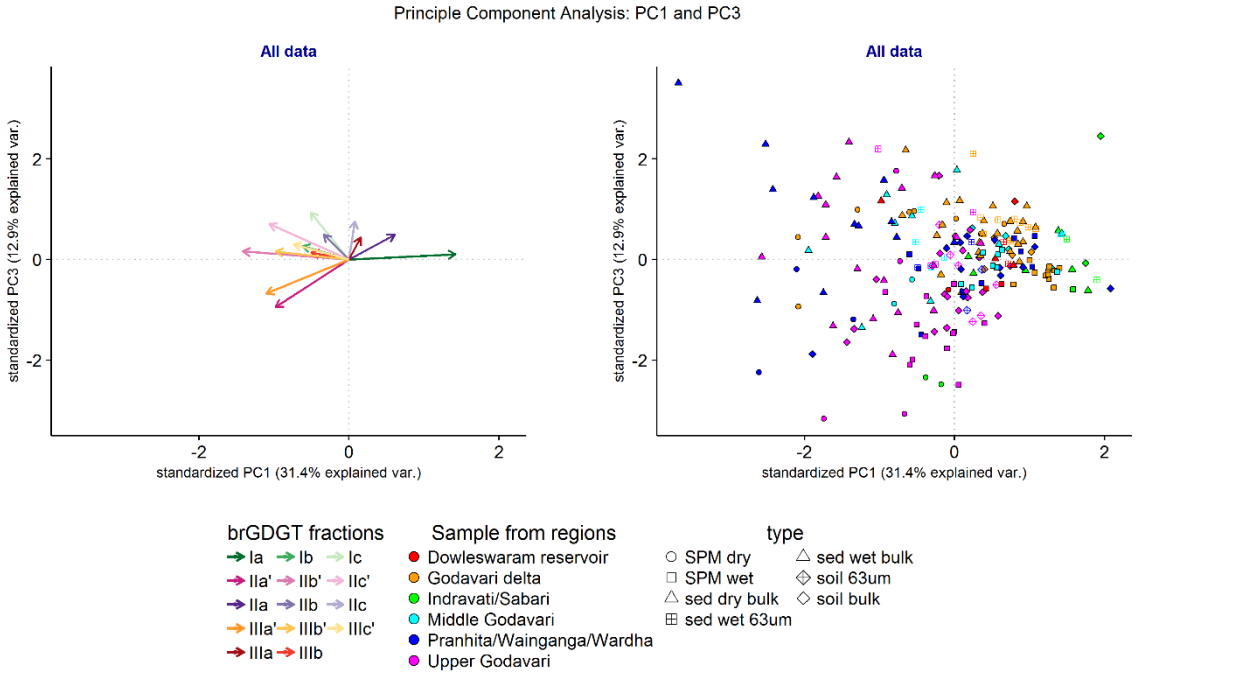

Figure 27 Results from the PCA analysis for all samples combined, plotted on the first and third principle component axes (PC1 and PC3, respectively).

4.5.1 Soils

The variance that is explained by the first three component axes (PC1-3) for bulk soil samples (PC1 and PC2 in ***Figure 28***, PC1 and PC3 in ***Figure 29***) added up to 74%. Also for this subset, the most important feature on PC1 was the inverse relationship between the fraction of brGDGT Ia (and Ic to a lesser degree) on one hand, and mainly the fractions of 6-Me brGDGTs IIa', IIb' IIIa' and IIIb' (r^2 with the fraction of Ia for these 6-Me brGDGT fractions was 0.77, 0.86, 0.68 and 0.39, respectively) on the other hand. On PC2 the highest negative loadings were brGDGT fractions IIa (IIb to a smaller degree), IIIa and IIIb (r^2 = 0.44 and 0.51, for IIa and IIIa, IIIa and IIIb, respectively). The highest positive loadings on PC2 were brGDGT fractions Ib and IIa'.

Bulk soil samples from the Godavari upstream areas (Upper Godavari and northern region) showed diffusive scores, although, generally Upper Godavari samples seemed to score more negatively on PC1, while northern area bulk soil samples scored more positively. Bulk soil samples from other regions showed a strong clustering pattern: samples from the eastern region scored relatively high on PC1 and relatively low on PC2, whereas samples from the Godavari delta and Middle Godavari regions scored low on both PC1 and PC2. A similar trend was expressed on PC3, Godavari delta and IS bulk soil samples clustered on relatively positive and negative scores, respectively, whereas upstream samples showed a large amount of scatter.

The soil sample scores show that the distribution of brGDGTs is highly affected by region. Downstream along the Godavari river, an increasing dominance of brGDGT Ia is present in soil samples at the expense of mostly 6-Me brGDGTs and brGDGTs Ib and Ic to a smaller degree.

4.5.2 SPM

The PCA for SPM samples was performed separately for dry and monsoon seasons (PC1 and PC2 in ***Figure 28***, PC1 and PC3 in ***Figure 29***). The variance that is explained by the first three

component axes (PC1-3) for SPM samples was 65% and 69% for the dry and monsoon seasons, respectively.

For **monsoon season** SPM samples, PC1 exhibited an inverse relationship between negatively scoring brGDGT fractions Ia and IIa (and IIIa to a lesser degree) on one hand, and positively scoring brGDGT fractions Ib, and 6-Me brGDGTs IIa', IIb', IIIa', in a similar fashion to soil samples. Strikingly, the negatively scoring brGDGTs were all brGDGTs containing no pentane moieties, whereas brGDGTs containing one or two pentane moieties scored positively, so possibly PC1 is capturing pH. The strong inverse relationship of brGDGT Ia to these 6-Me brGDGTs showed an equally high correlation in monsoon season SPM samples (r^2= 0.84, 0.78 and 0.79, respectively).

PC2 on the other hand, was determined by positive scores of brGDGTs Ib and IIb' (and Ia, Ic and IIc' to a lesser degree) and negative scores of brGDGTs IIIa, IIa, IIb and IIc (and IIIa', IIa' and IIb' to a lesser degree).

Finally, PC3 showed negative scores for brGDGTs IIa' and IIIa', while mainly the bicyclic brGDGTs (i.e. Ic, IIc, IIc', IIIc and IIIc') scored positively.

The strong similarities that monsoon season SPM showed to soil samples are indicative that these brGDGTs are of soil origin. The spatial distribution associated with SPM samples showed a distinctive pattern. The Upper Godavari and northern area samples showed major spreading, a similar pattern to that of the soil samples. Moving downstream, lower scores are observed, associated with the increasing fractional abundance of brGDGT Ia. This trend maximized in the eastern Indravati/Sabari area, which scored most negatively. The Godavari Delta region samples were an intermediate in this trend, although lop-sided toward the negative side, suggesting that during the monsoon season, the delta SPM signal is mainly driven by the contributions of the eastern area with minor influence of the rest of the catchment.

For **dry season** SPM samples, PC1 is determined by an inverse relationship between IIa' and IIIa' on one hand (IIb' and IIIb' to a lesser degree) and the tetramethylated brGDGTs and IIa on the other hand. Herein, the positively scoring brGDGTs were Ia, Ib, Ic and IIa and the negatively scoring were IIa' and IIIa' (correlation with these last two brGDGTs was r^2 = 0.50; 0.45; 0.72; 0.22 and r^2 = 0.53; 0.41; 0.60; 0.32, respectively). Strikingly, the 5-Me and 6-Me brGDGTs showed opposing behaviour.

PC2 was described by negative scores of brGDGTs IIb' and IIc', whereas PC3 was mainly determined by positive scores of brGDGTs IIIa and IIc.

A pattern in spatial distribution seemed to be absent; there was no evident clustering of samples.

That the dry season SPM brGDGT distribution is distinctly different from the monsoon SPM is further amplified by its differentiation from the soil samples. Whereas the monsoon SPM brGDGT signal closely mimicked that of soils, the SPM signal in the dry season does not. Rather, a high spreading on the PCA plot shows the low variability between samples (also see Distribution of brGDGTs 4.4) It suggests that source of brGDGTs of dry season SPM may not be of soil origin.

Other studies have found similar discrepancies between brGDGT distributions of SPM and soils, particularly in river systems where aquatic production of brGDGTs may occur. For example, in peat bogs (De Jonge et al, 2013) and the Yensei River (De Jonge et al., 2014b) the contribution of aquatic brGDGTs production was proposed. The low-water discharge of the Godavari River, as exhibited during dry season, may play a role in favouring aquatic production during discharge.

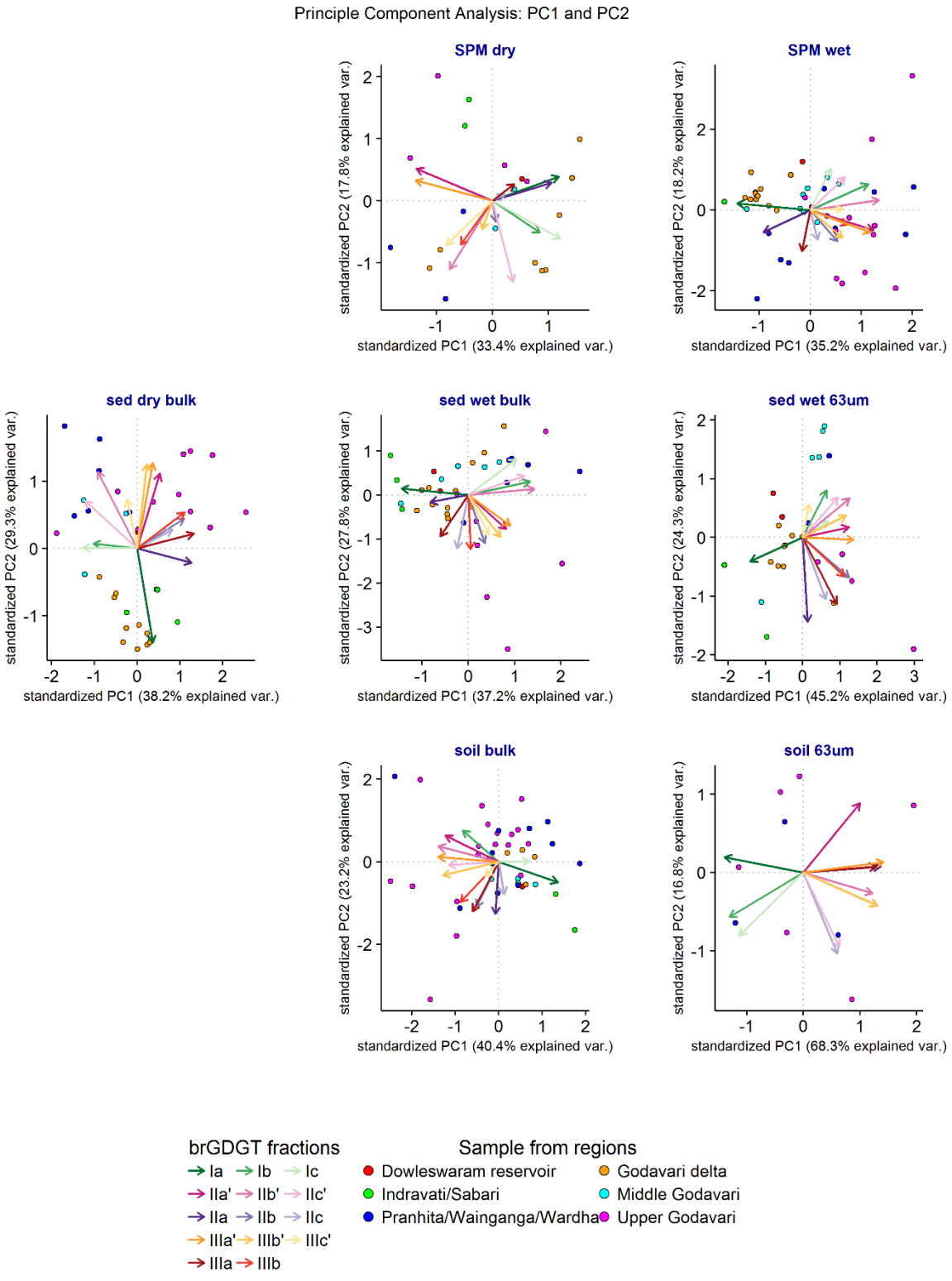

Figure 28 PCA analysis for each sample type and sampling season, plotted on the first and second principle component axis.

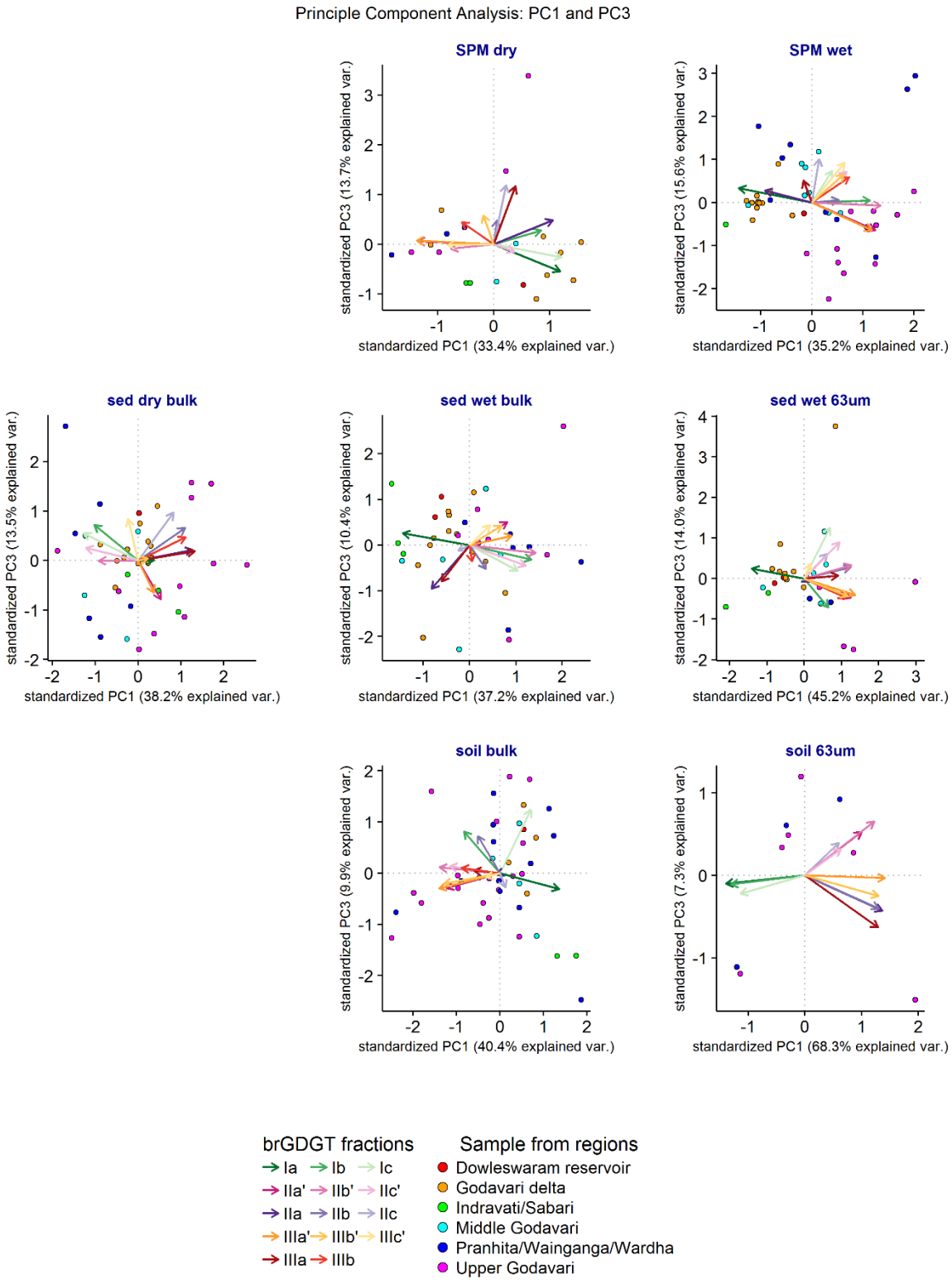

Figure 29 PCA analysis for each sample type and sampling season, plotted on the first and third principle component axis.

4.5.3 River sediment

The PCA for river sediment samples (PC1 and PC2 in ***Figure 28***, PC1 and PC3 in ***Figure 29***) was performed separately for dry and monsoon seasons. The variance that is explained by the first three component axes (PC1-3) for river sediment samples was 81% and 75% for the dry and monsoon seasons, respectively.

For river sediments from the **monsoon season,** the same negative correlation between brGDGT Ia on the one hand versus IIa', IIb', IIc' and IIIa', (6-Me isomers), Ib and additionally Ic (r^2 = 0.37; 0.87; 0.55; 0.48; 0.72; 0.42) on the other hand was noted, as for wet season SPM and bulk soils.

PC1 was mainly determined by brGDGT Ia and smaller contributions of IIa and IIIa on the one side (scoring negatively) and the above mentioned 6-Me isomers on the other side (scoring positively). PC2 featured brGDGTs IIa, IIb, IIc, IIIa, IIIb, IIa', IIIa', IIIb' and IIIc' in negative direction, and Ib, Ic and IIc' in positive direction. PC3 was mainly characterized by a negative score of brGDGTs IIa and IIIa.

Remarkably, the brGDGT distribution of monsoon season sediments nearly identical to the monsoon season SPM brGDGT distribution (and soil to a somewhat lesser degree), suggesting a common origin. Region seems to be an important factor for the sample score on PC1: Indravati/Sabari samples score most negative, whereas Upper Godavari and northern area samples score most positive. Godavari Delta samples also score negative, although to a smaller degree. This suggests that the river sediment deposited in the Godavari delta is an integrated signal of mostly IS and Middle Godavari origin and the Upper Godavari area seems to contribute minimally during the monsoon season.

During the **dry season**, for river sediments, brGDGTs Ib, Ic, IIb'and IIc' were negatively correlated with IIa, IIb, IIc, IIIa, IIIb on PC1. PC2 showed an inverse correlation between Ia

(scoring negatively) and brGDGTs IIa', IIb', IIc', IIIa', IIIb' and IIIc' (scoring positively) on the other hand (r^2= 0.39; 0.72; 0.42; 0.53; 0.39; 0.13,). PC3 exhibited IIa' and IIIa' in negative direction versus all other brGDGTs in positive direction. The geographical distribution of different samples had a marked effect on the scores on the PCA. The Upper Godavari and northern area samples scored positively on PC2, associated with predominance of 6-Me brGDGTs Indravati/Sabari and Godavari Delta samples, however, scored negatively on PC2, associated with brGDGT Ia. The Middle Godavari showed an intermediate score.

Comparing the dry season river sediments with the SPM in this season, there are similarities in brGDGT distributions, highlighted by the anti-correlation between tetramethylated brGDGTs on one hand, and 6-Me penta- and hexamethylated brGDGTs on the other. However, dry season bulk sediments show no strong resemblance to PCA distribution patterns of soils, indicating that soil input is small compared to monsoon season and its brGDGT distribution is rather the mixed result of soil input and aquatic production.

5 Discussion

5.1 Land-sea transport of SOC

The Godavari River sediment transport is strongly monsoon-driven, which is especially evident from its two-orders-of-magnitude higher sediment loading in the delta region during the monsoon season months. However, the spatially different precipitation regime in the catchment area is driving preferential SOC transport from the eastern side of the catchment. The brGDGT distribution in soils is mimicked by the SPM brGDGT signal in this region, all the way to the delta, suggesting that SOC discharged to the Bay of Bengal has its provenance mainly in this area. Changes in the fraction of brGDGT Ia in SPM (which is the most dominant brGDGT in the Godavari soils) show to capture the degree of soil input best (***Figure 30***), while a high contribution of 6-Me brGDGTs suggests a lack of soil input and relative increase of primary production (***Figure 31***).

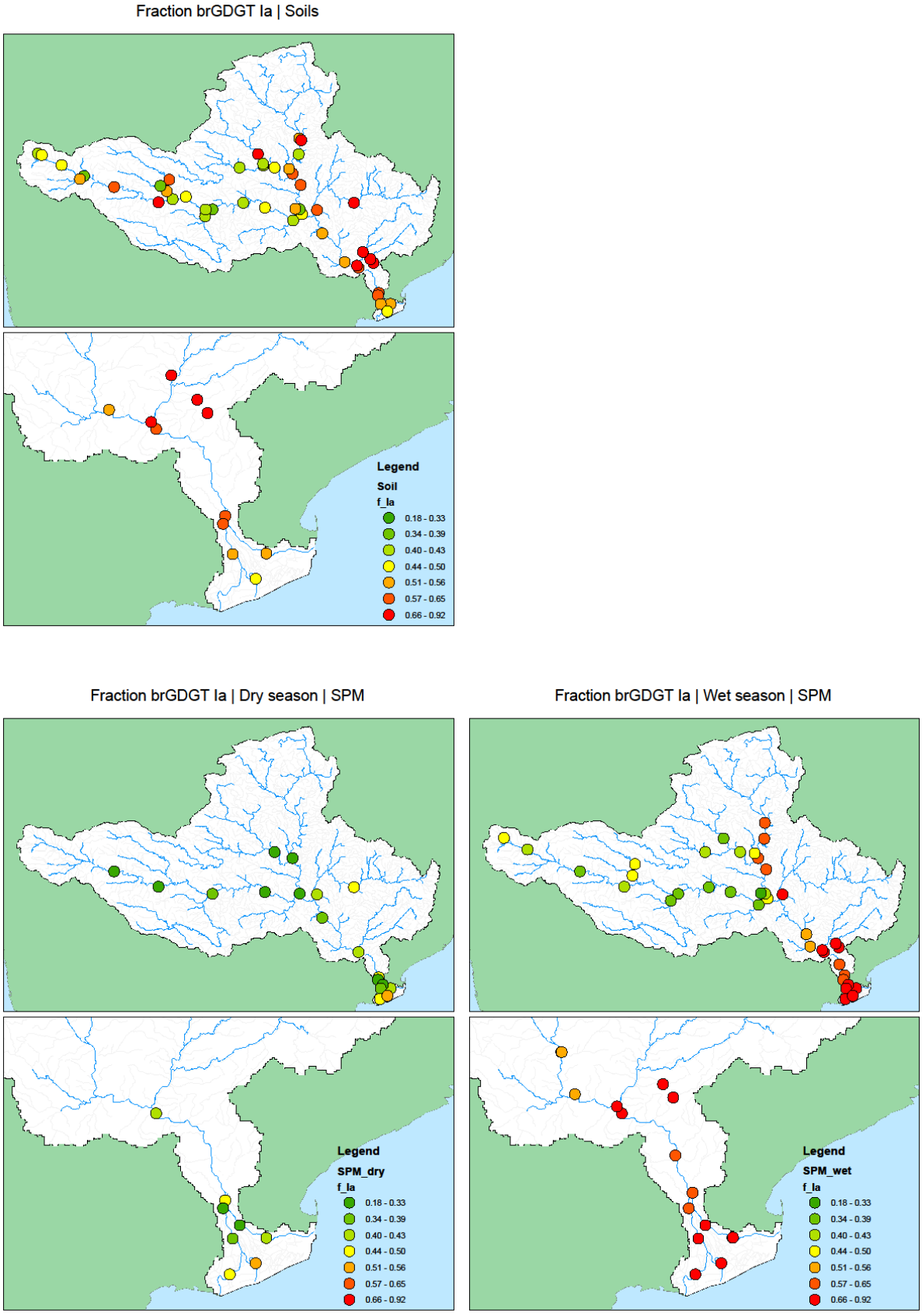

Figure 30 The fraction of brGDGT Ia in Godavari soils (upper) and SPM (lower) in the dry (left) and monsoon (right) season

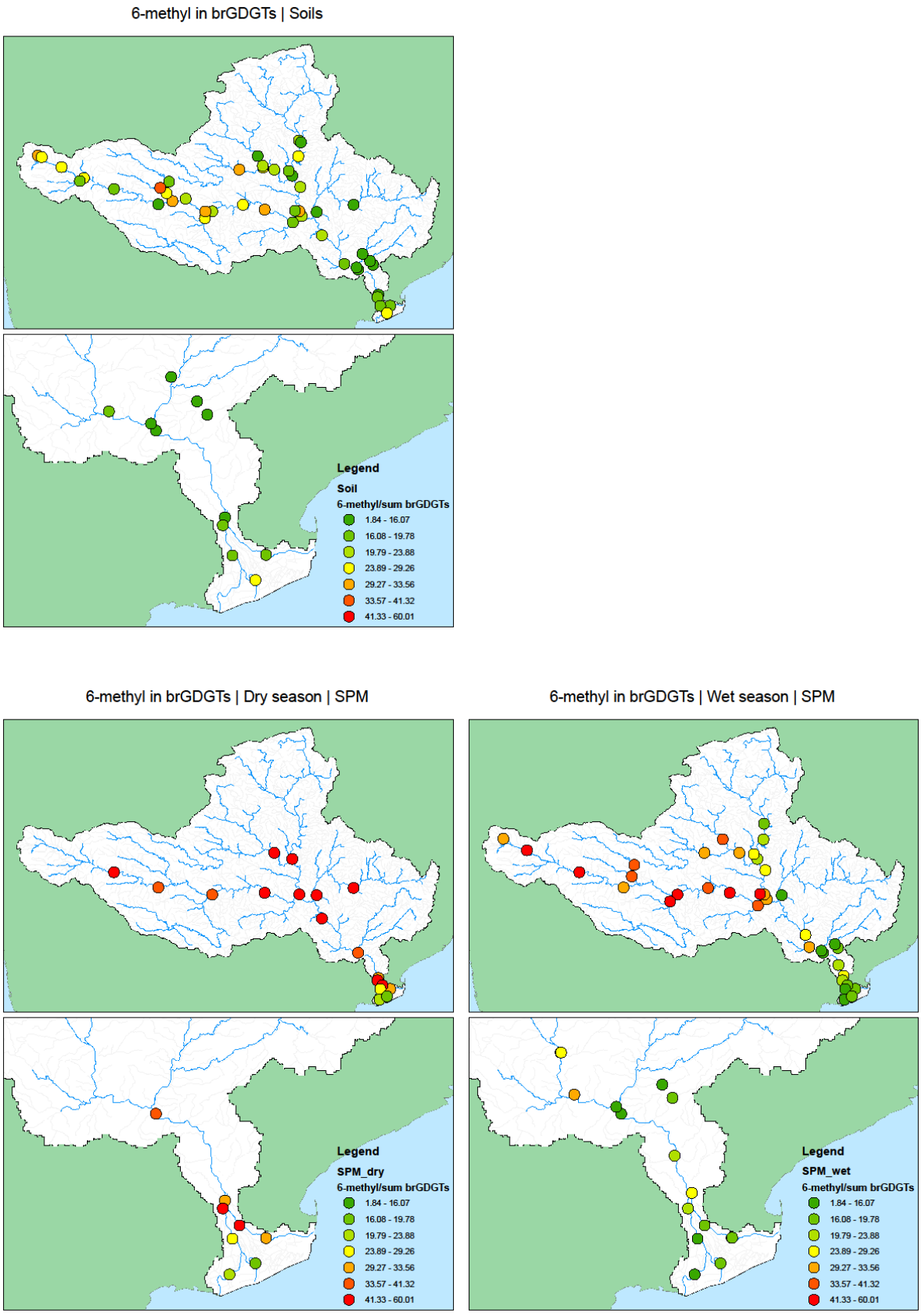

Figure 31 The relative abundance (%) of 6-methyl isomers in Godavari soils (upper) and SPM during dry (left) and monsoon (right) season

5.2 Role of aquatic brGDGT production

For the Godavari catchment area, aquatic in situ production seems to play a role in the finally discharged brGDGT signal. During the dry season, river SPM is characterized by an increased relative abundance of the isomers of penta- and hexamethylated brGDGTs, and this is a catchment-wide phenomenon. For the western area of the catchment, this seems to be also valid during the monsoon season, most likely because of restricted soil erosion due to limited precipitation in this area. The SPM-based pH reconstruction of the eastern area, that is characterized by soil erosion during the monsoon season, does not show the soil-characteristic acidic values during the dry season. Rather, they show values in line with the rest of the catchment area. The contribution of 6-Me isomers equally increases during the dry season, in this region This suggests that rather than soil pH, the brGDGT distribution in SPM captures water pH during the dry season and thus these brGDGTs most likely has an aquatic origin.

In the Yenisei River (Siberia), a similar discrepancy between SPM and soil was shown in 6-Me isomers (De Jonge et al., 2014b). While the degree of isomerisation (% 6-Me isomers) thus seems to be related to aquatic production, their origin is not exclusively aquatic, as they abundance increases substantially with pH in more alkaline soils (De Jonge et al., 2014a). Furthermore, the study of Freymond et al. (2017) of SOC transport in the Danube River, found relatively high contributions of soil-derived 6-Me brGDGTs. Consequently, the separation of soil and aquatic-derived brGDGTs in modern systems cannot be based solely on the contribution of 6-Me brGDGTs.

5.3 Use of brGDGTs in paleoclimate reconstructions

Care should be advised in employing the brGDGT based climate proxies here reported (BIT index, MAT_{mr} and reconstructed pH using CBT').

Firstly, for the BIT index, the previous assumption in some paleo-environment reconstructions that the source of brGDGTs and isoGDGT crenarchaeol is exclusive is crucially inappropriate

under certain environmental conditions. In the Godavari catchment area, crenarchaeol is also relatively abundant in soils. This seems to be related to their relatively high soil pH, and this phenomenon was equally reported by Kim et al., 2010 for the Têt River catchment area. Therefore, applying the BIT index near river fans characterized by alkaline soils in their catchment area seems inadvisable as its value may not accurately describe the relative contribution of terrestrial organic matter, but is rather skewed by soil-derived crenarchaeol.

Secondly, for the MAT_{mr}, discussed previously by Naafs, et al. (2017), the MAT_{mr} proxy seems to be limited to a maximum temperature of ~25 °C. In the Godavari catchment, this is further complicated by the arid nature of the Godavari soils and their relatively high content of 6-Me brGDGTs.

Thirdly, for the CBT' based pH reconstruction, the proxy captures regional pH variations in the catchment area in both soils and river water, but underestimates pH by approximately 1-1.5 unit. This seems to be an artefact of the CBT' calibration to soil pH, as the calibration of De Jonge et al. (2014a) seems to become less accurate for alkaline soils.

Finally, proxy values from marine sediment do not always fully represent the environmental conditions of a river's upstream catchment. SOC can be preferentially transported from a single region, as the case in the Godavari catchment.

6 Conclusions

The full suite of 15 brGDGT compounds have been assessed in the Godavari catchment area (India), in soils, but also in dry and monsoon season SPM and river sediments.

The brGDGT distribution in soils and SPM could capture changes in environmental conditions (pH, temperature) in soils and river water. However, both the absolute value of pH and temperature were locally underestimated substantially. For temperature, the MAT_{mr} proxy is known to be limited to temperatures of ~25 °C. In addition, the arid nature of the western Godavari seemed to cause the proxy to further deviate from actual MAAT.

The physical properties of river water, sediment loading and brGDGT distribution showed that the transport of soil organic matter (characterized by a relatively high abundance of brGDGT Ia) to the Bay of Bengal is primarily associated with the monsoon season, whereas during dry season the brGDGT distribution is characterized by aquatic production of mostly 6-methyl isomers of penta- and hexamethylated brGDGTs (especially brGDGT IIa' and IIIa'). Moreover, variation in the degree of isomerisation (i.e. % 6-Me) seems to be able to capture the relative contribution of soil-derived brGDGTs and aquatic production in the Godavari River system. However, care should be advised when using 6-Me brGDGT isomers as indicator for aquatic production in general, as their origin is not exclusively from aquatic environments, they were also found in relatively high abundance in some of the alkaline soils, both in this study and the global dataset of De Jonge et al. (2014a).

The precipitation regime in the Godavari catchment area is driving the transport and provenance of soil organic matter that was finally discharged. The Indravati/Sabari tributaries, affected most by heavy monsoon rainfall, contributes most to the SOC discharge in the delta. Whereas in situ derived brGDGTs characterize the Godavari River discharge during dry season, soil-derived brGDGTs dominate the Godavari discharge during the wet season. Although brGDGTs can adequately be employed to trace SOC through a catchment, the processes affecting their fate during transport need further investigation before their distribution can be effectively and accurately applied in paleo-environmental reconstructions, as without a reference on the provenance of SOC it remains impossible to segregate the soil-derived brGDGT signal from transformations during transport.

References

Aufdenkampe, A. K., Mayorga, E., Raymond, P. A., Melack, J. M., Doney, S. C., Alin, S. R., ... & Yoo, K. (2011). Riverine coupling of biogeochemical cycles between land, oceans, and atmosphere. *Frontiers in Ecology and the Environment*, *9*(1), 53-60.

Bendle, J. A., Weijers, J. W., Maslin, M. A., Sinninghe Damsté, J. S., Schouten, S., Hopmans, E. C., ... & Pancost, R. D. (2010). Major changes in glacial and Holocene terrestrial temperatures and sources of organic carbon recorded in the Amazon fan by tetraether lipids. *Geochemistry, Geophysics, Geosystems*, *11*(12).

Biksham, G., & Subramanian, V. (1988). Sediment transport of the Godavari River basin and its controlling factors. *Journal of Hydrology*, 101(1-4), 275-290.

Blaga, C. I., Reichart, G. J., Heiri, O., & Damsté, J. S. S. (2009). Tetraether membrane lipid distributions in water-column particulate matter and sediments: a study of 47 European lakes along a north–south transect. *Journal of Paleolimnology*, *41*(3), 523-540.

Cole, J. J., Prairie, Y. T., Caraco, N. F., McDowell, W. H., Tranvik, L. J., Striegl, R. G., ... & Melack, J. (2007). Plumbing the global carbon cycle: integrating inland waters into the terrestrial carbon budget. *Ecosystems*, *10*(1), 172-185.

Damsté, J. S. S. (2016). Spatial heterogeneity of sources of branched tetraethers in shelf systems: The geochemistry of tetraethers in the Berau River delta (Kalimantan, Indonesia). *Geochimica et Cosmochimica Acta*, *186*, 13-31.

Damsté, J. S. S., Hopmans, E. C., Pancost, R. D., Schouten, S., & Geenevasen, J. A. (2000). Newly discovered non-isoprenoid glycerol dialkyl glycerol tetraether lipids in sediments. *Chemical Communications*, (17), 1683-1684.

Damsté, J. S. S., Ossebaar, J., Abbas, B., Schouten, S., & Verschuren, D. (2009). Fluxes and distribution of tetraether lipids in an equatorial African lake: constraints on the application of the TEX 86 palaeothermometer and BIT index in lacustrine settings. *Geochimica et Cosmochimica Acta*, *73*(14), 4232-4249.

Damsté, J. S. S., Ossebaar, J., Schouten, S., & Verschuren, D. (2012). Distribution of tetraether lipids in the 25-ka sedimentary record of Lake Challa: extracting reliable TEX 86 and MBT/CBT palaeotemperatures from an equatorial African lake. *Quaternary Science Reviews*, 50, 43-54.

Dang, X., Yang, H., Naafs, B. D. A., Pancost, R. D., & Xie, S. (2016). Evidence of moisture control on the methylation of branched glycerol dialkyl glycerol tetraethers in semi-arid and arid soils. *Geochimica et Cosmochimica Acta*, *189*, 24-36.

De Jonge, C., Hopmans, E. C., Stadnitskaia, A., Rijpstra, W. I. C., Hofland, R., Tegelaar, E., & Damsté, J. S. S. (2013). Identification of novel penta-and hexamethylated branched glycerol dialkyl glycerol tetraethers in peat using HPLC–MS 2, GC–MS and GC–SMB-MS. *Organic geochemistry*, *54*, 78-82.

De Jonge, C., Hopmans, E. C., Zell, C. I., Kim, J. H., Schouten, S., & Damsté, J. S. S. (2014a). Occurrence and abundance of 6-methyl branched glycerol dialkyl glycerol tetraethers in soils: Implications for palaeoclimate reconstruction. *Geochimica et Cosmochimica Acta*, *141*, 97-112.

De Jonge, C., Stadnitskaia, A., Cherkashov, G., & Damsté, J. S. S. (2016). Branched glycerol dialkyl glycerol tetraethers and crenarchaeol record post-glacial sea level rise and shift in source of terrigenous brGDGTs in the Kara Sea (Arctic Ocean). *Organic Geochemistry*, *92*, 42-54.

De Jonge, C., Stadnitskaia, A., Fedotov, A., & Damsté, J. S. S. (2015a). Impact of riverine suspended particulate matter on the branched glycerol dialkyl glycerol tetraether composition of lakes: The outflow of the Selenga River in Lake Baikal (Russia). *Organic Geochemistry*, *83*, 241-252.

De Jonge, C., Stadnitskaia, A., Hopmans, E. C., Cherkashov, G., Fedotov, A., & Damsté, J. S. S. (2014b). In situ produced branched glycerol dialkyl glycerol tetraethers in suspended particulate matter from the Yenisei River, Eastern Siberia. *Geochimica et Cosmochimica Acta*, *125*, 476-491.

De Jonge, C., Stadnitskaia, A., Hopmans, E. C., Cherkashov, G., Fedotov, A., Streletskaya, I. D., ... & Damsté, J. S. S. (2015b). Drastic changes in the distribution of branched tetraether lipids in suspended matter and sediments from the Yenisei River and Kara Sea (Siberia): Implications for the use of brGDGT-based proxies in coastal marine sediments. *Geochimica et Cosmochimica Acta*, *165*, 200-225.

De Rosa, M., & Gambacorta, A. (1988). The lipids of archaebacteria. *Progress in lipid research*, *27*(3), 153-175.

Dean, W. E., & Gorham, E. (1998). Magnitude and significance of carbon burial in lakes, reservoirs, and peatlands. *Geology*, 26(6), 535-538.

Deshpande, N. R., Kothawale, D. R., & Kulkarni, A. (2016). Changes in climate extremes over major river basins of India. *International Journal of Climatology*, *36*(14), 4548-4559.

Dirghangi, S. S., Pagani, M., Hren, M. T., & Tipple, B. J. (2013). Distribution of glycerol dialkyl glycerol tetraethers in soils from two environmental transects in the USA. *Organic Geochemistry*, *59*, 49-60.

Donders, T. H., Weijers, J. W. H., Munsterman, D. K., Kloosterboer-van Hoeve, M. L., Buckles, L. K., Pancost, R. D., ... & Brinkhuis, H. (2009). Strong climate coupling of terrestrial and marine environments in the Miocene of northwest Europe. *Earth and Planetary Science Letters*, *281*(3), 215-225.

FAO/IIASA/ISRIC/ISS-CAS/JRC, 2009. Harmonized World Soil Database (version 1.1). FAO, Rome, Italy and IIASA, Laxenburg, Austria.

Freymond, C. V., Peterse, F., Fischer, L. V., Filip, F., Giosan, L., & Eglinton, T. I. (2017). Branched GDGT signals in fluvial sediments of the Danube River basin: Method comparison and longitudinal evolution. *Organic Geochemistry*, *103*, 88-96.

Galy, V., & Eglinton, T. (2011). Protracted storage of biospheric carbon in the Ganges-Brahmaputra basin. *Nature Geoscience*, *4*(12), 843.

Galy, V., France-Lanord, C., & Lartiges, B. (2008). Loading and fate of particulate organic carbon from the Himalaya to the Ganga–Brahmaputra delta. *Geochimica et Cosmochimica Acta*, *72*(7), 1767-1787.

Galy, V., France-Lanord, C., Beyssac, O., Faure, P., Kudrass, H., & Palhol, F. (2007). Efficient organic carbon burial in the Bengal fan sustained by the Himalayan erosional system. *Nature*, *450*(7168), 407.

Gat, J. R. (1996). Oxygen and hydrogen isotopes in the hydrologic cycle. Annual Review of Earth and Planetary Sciences, 24(1), 225-262.

Gonfiantini, R. (1978). Standards for sTable isotope measurements in natural compounds. *Nature*, *271*(5645), 534-536.

Hanna, A. J., Shanahan, T. M., & Allison, M. A. (2016). Distribution of branched GDGTs in surface sediments from the Colville River, Alaska: Implications for the MBT'/CBT paleothermometer in Arctic marine sediments. *Journal of Geophysical Research: Biogeosciences*, *121*(7), 1762-1780.

Hopmans, E. C., Schouten, S., & Damsté, J. S. S. (2016). The effect of improved chromatography on GDGT-based palaeoproxies. *Organic Geochemistry*, *93*, 1-6.

Hopmans, E. C., Weijers, J. W., Schefuß, E., Herfort, L., Damsté, J. S. S., & Schouten, S. (2004). A novel proxy for terrestrial organic matter in sediments based on branched and isoprenoid tetraether lipids. *Earth and Planetary Science Letters*, *224*(1), 107-116.

Huguet, C., Hopmans, E. C., Febo-Ayala, W., Thompson, D. H., Damsté, J. S. S., & Schouten, S. (2006). An improved method to determine the absolute abundance of glycerol dibiphytanyl glycerol tetraether lipids. *Organic Geochemistry*, *37*(9), 1036-1041.

Jaffé, R., Mead, R., Hernandez, M. E., Peralba, M. C., & DiGuida, O. A. (2001). Origin and transport of sedimentary organic matter in two subtropical estuaries: a comparative, biomarker-based study. *Organic Geochemistry*, 32(4), 507-526.

Jeelani, G., Kumar, U. S., & Kumar, B. (2013). Variation of δ 18 O and δD in precipitation and stream waters across the Kashmir Himalaya (India) to distinguish and estimate the seasonal sources of stream flow. *Journal of hydrology*, 481, 157-165.

Kim, J. H., Ludwig, W., Buscail, R., Dorhout, D., & Damsté, J. S. S. (2015). Tracing tetraether lipids from source to sink in the Rhône River system (NW Mediterranean). *Frontiers in Earth Science*, *3*, 22-p.

Kim, J. H., Talbot, H. M., Zarzycka, B., Bauersachs, T., & Wagner, T. (2011). Occurrence and abundance of soil-specific bacterial membrane lipid markers in the Têt watershed (southern France): Soil-specific BHPs and branched GDGTs. *Geochemistry, Geophysics, Geosystems*, *12*(2).

Kim, J. H., Zarzycka, B., Buscail, R., Peterse, F., Bonnin, J., Ludwig, W., ... & Sinninghe Damsté, J. S. (2010). Contribution of river-borne soil organic carbon to the Gulf of Lions (NW Mediterranean). *Limnology and oceanography*, 55(2), 507-518.

Kirtman, B., S.B. Power, J.A. Adedoyin, G.J. Boer, R. Bojariu, I. Camilloni, F.J. Doblas-Reyes, A.M. Fiore, M. Kimoto, G.A. Meehl, M. Prather, A. Sarr, C. Schär, R. Sutton, G.J. van Oldenborgh, G. Vecchi and H.J. Wang, 2013: Near-term Climate Change: Projections and Predictability. In: Climate Change 2013: The Physical Science Basis. *Contribution of Working Group I to the Fifth Assessment Report of the Intergovernmental Panel on Climate Change* [Stocker, T.F., D. Qin, G.-K. Plattner, M. Tignor, S.K. Allen, J. Boschung, A. Nauels, Y. Xia, V. Bex and P.M. Midgley (eds.)]. Cambridge University Press, Cambridge, United Kingdom and New York, NY, USA.

Komada, T., Anderson, M. R., & Dorfmeier, C. L. (2008). Carbonate removal from coastal sediments for the determination of organic carbon and its isotopic signatures, δ13C and Δ14C: comparison of fumigation and direct acidification by hydrochloric acid. *Limnology and Oceanography: Methods*, *6*(6), 254-262.

Kumar, R., Goel, N. K., Chatterjee, C., & Nayak, P. C. (2015). Regional flood frequency analysis using soft computing techniques. *Water resources management*, *29*(6), 1965-1978.

Kusch, S., Rethemeyer, J., Schefuß, E., & Mollenhauer, G. (2010). Controls on the age of vascular plant biomarkers in Black Sea sediments. *Geochimica et Cosmochimica Acta*, 74(24), 7031-7047.

Li, Z., Peterse, F., Wu, Y., Bao, H., Eglinton, T. I., & Zhang, J. (2015). Sources of organic matter in Changjiang (Yangtze River) bed sediments: preliminary insights from organic geochemical proxies. *Organic Geochemistry*, *85*, 11-21.

Lupker, M., France-Lanord, C., Lavé, J., Bouchez, J., Galy, V., Métivier, F., ... & Mugnier, J. L. (2011). A Rouse-based method to integrate the chemical composition of river sediments: Application to the Ganga basin. *Journal of Geophysical Research: Earth Surface*, *116*(F4).

Mead, R., Xu, Y., Chong, J., & Jaffé, R. (2005). Sediment and soil organic matter source assessment as revealed by the molecular distribution and carbon isotopic composition of n-alkanes. *Organic Geochemistry*, 36(3), 363-370.

Menges, J., Huguet, C., Alcañiz, J. M., Fietz, S., Sachse, D., & Rosell-Melé, A. (2014). Influence of water availability in the distributions of branched glycerol dialkyl glycerol tetraether in soils of the Iberian Peninsula. *Biogeosciences*, *11*(10), 2571-2581.

Pearson, A., Huang, Z., Ingalls, A. E., Romanek, C. S., Wiegel, J., Freeman, K. H., ... & Zhang, C. L. (2004). Nonmarine crenarchaeol in Nevada hot springs. *Applied and Environmental Microbiology*, *70*(9), 5229-5237.

Peters, K. E., Walters, C. C., & Moldowan, J. M. (2005). *The biomarker guide,* (Vol. 1). Cambridge University Press.

Peterse, F., van der Meer, J., Schouten, S., Weijers, J. W., Fierer, N., Jackson, R. B., ... & Damsté, J. S. S. (2012). Revised calibration of the MBT–CBT paleotemperature proxy based on branched tetraether membrane lipids in surface soils. *Geochimica et Cosmochimica Acta*, *96*, 215-229.

Rao, K. N., Saito, Y., Nagakumar, K. C. V., Demudu, G., Rajawat, A. S., Kubo, S., & Li, Z. (2015). Palaeogeography and evolution of the Godavari delta, east coast of India during the Holocene: an example of wave-dominated and fan-delta settings. *Palaeogeography, Palaeoclimatology, Palaeoecology*, *440*, 213-233.

Ray, S.K., Reddy, R.S. and Budihal, S.L. 1997. Vertisols and associated soils development and lithological discontinuity in coastal Godavari delta region. J. *Indian Soc. Coastal Agri*. Res. XV:1-14.

Regnier, P., Friedlingstein, P., Ciais, P., Mackenzie, F. T., Gruber, N., Janssens, I. A., ... & Arndt, S. (2013). Anthropogenic perturbation of the carbon fluxes from land to ocean. *Nature geoscience*, *6*(8), 597.

Sarma, V. V. S. S., Kumar, N. A., Prasad, V. R., Venkataramana, V., Appalanaidu, S., Sridevi, B., ... & Rao, G. D. (2011). High CO2 emissions from the tropical Godavari estuary (India) associated with monsoon river discharges. *Geophysical Research Letters*, 38(8).

Sarmiento, J. L., & Gruber, N. (2002). Sinks for anthropogenic carbon. Physics today, 55(8), 30-36. Chicago

Schouten, S., Baas, M., Hopmans, E. C., & Damsté, J. S. S. (2008). An unusual isoprenoid tetraether lipid in marine and lacustrine sediments. *Organic Geochemistry*, *39*(8), 1033-1038.

Schouten, S., Hopmans, E. C., & Damsté, J. S. S. (2013). The organic geochemistry of glycerol dialkyl glycerol tetraether lipids: a review. *Organic geochemistry*, *54*, 19-61.

Tierney, J. E., & Russell, J. M. (2009). Distributions of branched GDGTs in a tropical lake system: implications for lacustrine application of the MBT/CBT paleoproxy. Organic Geochemistry, 40(9), 1032-1036.

Tierney, J. E., Schouten, S., Pitcher, A., Hopmans, E. C., & Damsté, J. S. S. (2012). Core and intact polar glycerol dialkyl glycerol tetraethers (GDGTs) in Sand Pond, Warwick, Rhode Island (USA): Insights into the origin of lacustrine GDGTs. *Geochimica et Cosmochimica Acta*, 77, 561-581.

Tripti, M., Lambs, L., Gurumurthy, G. P., Moussa, I., Balakrishna, K., & Chadaga, M. D. (2016). Water circulation and governing factors in humid tropical river basins in the central Western Ghats, Karnataka, India. *Rapid Communications in Mass Spectrometry*, 30(1), 175-190.

Voort, T. S. van den., Hagedorn, F., McIntyre, C., Zell, C., Walthert, L., Schleppi, P., ... & Eglinton, T. I. (2016). Variability in 14 C contents of soil organic matter at the plot and regional scale across climatic and geologic gradients. *Biogeosciences*, *13*(11), 3427-3439

Wacker, L., Němec, M., & Bourquin, J. (2010). A revolutionary graphitisation system: fully automated, compact and simple. *Nuclear Instruments and Methods in Physics Research Section B: Beam Interactions with Materials and Atoms*, *268*(7), 931-934.

Wang, H., Liu, W., Zhang, C. L., Wang, Z., Wang, J., Liu, Z., & Dong, H. (2012). Distribution of glycerol dialkyl glycerol tetraethers in surface sediments of Lake Qinghai and surrounding soil. *Organic Geochemistry*, *47*, 78-87.

Weijers, J. W., Schouten, S., Hopmans, E. C., Geenevasen, J. A., David, O. R., Coleman, J. M., ... & Sinninghe Damsté, J. S. (2006b). Membrane lipids of mesophilic anaerobic bacteria thriving in peats have typical archaeal traits. *Environmental Microbiology*, *8*(4), 648-657.

Weijers, J. W., Schouten, S., Spaargaren, O. C., & Damsté, J. S. S. (2006a). Occurrence and distribution of tetraether membrane lipids in soils: implications for the use of the TEX 86 proxy and the BIT index. *Organic Geochemistry*, *37*(12), 1680-1693

Weijers, J. W., Schouten, S., van den Donker, J. C., Hopmans, E. C., & Damsté, J. S. S. (2007). Environmental controls on bacterial tetraether membrane lipid distribution in soils. *Geochimica et Cosmochimica Acta*, *71*(3), 703-713.

Zachos, J., Pagani, M., Sloan, L., Thomas, E., & Billups, K. (2001). Trends, rhythms, and aberrations in global climate 65 Ma to present.*Science*, *292*(5517), 686-693.

Zell, C., Kim, J. H., Abril, G., Sobrinho, R. L., Dorhout, D., Moreira-Turcq, P., & Damsté, J. S. S. (2013b). Impact of seasonal hydrological variation on the distributions of tetraether lipids along the Amazon River in the central Amazon basin: implications for the MBT/CBT paleothermometer and the BIT index. *Frontiers in microbiology*, *4*.

Zell, C., Kim, J. H., Balsinha, M., Dorhout, D., Fernandes, C., Baas, M., & Sinninghe Damsté, J. S. (2014b). Transport of branched tetraether lipids from the Tagus River basin to the coastal ocean of the Portuguese margin: consequences for the interpretation of the MBT'/CBT paleothermometer. *Biogeosciences*, *11*(19), 5637-5655.

Zell, C., Kim, J. H., Hollander, D., Lorenzoni, L., Baker, P., Silva, C. G., ... & Damsté, J. S. S. (2014a). Sources and distributions of branched and isoprenoid tetraether lipids on the Amazon shelf and fan: Implications for the use of GDGT-based proxies in marine sediments. *Geochimica et Cosmochimica Acta*, *139*, 293-312.

Zell, C., Kim, J. H., Moreira-Turcq, P., Abril, G., Hopmans, E. C., Bonnet, M. P., ... & Damsté, J. S. S. (2013a). Disentangling the origins of branched tetraether lipids and crenarchaeol in the lower Amazon River: Implications for GDGT-based proxies. *Limnology and Oceanography*, *58*(1), 343-353.

Zhang, Y. G., Pagani, M., & Wang, Z. (2016). Ring Index: A new strategy to evaluate the integrity of TEX86 paleothermometry. *Paleoceanography*, *31*(2), 220-232.

7 Supplements

7.1 Digital data

All measured and calculated concentrations, fractions and indices are available in the supplementary Excel file.

7.2 Maps

For all indices described in ***3.4.3 GDGT-based proxy calculations***, distribution maps were made. These maps are available in pdf format in the accompanying archive file.